



Oxidative coupling of methane over unsupported and alumina-supported samaria catalysts



Trenton W. Elkins, Helena E. Hagelin-Weaver*

Department of Chemical Engineering, University of Florida, Gainesville, FL, United States

ARTICLE INFO

Article history:

Received 24 October 2012

Received in revised form 2 January 2013

Accepted 5 January 2013

Available online xxx

Keywords:

Samarium oxide nanoparticles

Alumina-supported samaria

Methane coupling activity and selectivity

XRD

XPS

ABSTRACT

Being the shortest unsaturated hydrocarbon, ethylene is a valuable feedstock gas for synthesizing longer chain hydrocarbon products. Using the oxidative coupling of methane to produce ethylene and ethane (C_2 products) has been studied extensively over the past few decades. In this work, samaria nanoparticles (NPs) and alumina-supported samaria catalysts were prepared using different methods (water/toluene reverse microemulsion, metal-oleate high temperature decomposition, and incipient-wetness impregnation followed by calcination) and various types of alumina supports (high and low surface area nanoparticle alumina [$n-Al_2O_3(+)$, $n-Al_2O_3(-)$] and a porous gamma alumina support [$\gamma-Al_2O_3$]). The highest product yields were obtained over Sm_2O_3 NPs synthesized using the metal-oleate high temperature decomposition and a nitrate precursor. Using a chloride precursor in the preparation of the Sm_2O_3 NPs resulted in less active and selective catalysts, and should be avoided. While the C_2 selectivities were lower over the Sm_2O_3/Al_2O_3 catalysts, the yield per gram of Sm_2O_3 were higher compared with the Sm_2O_3 NPs. The best supported catalyst was the $Sm_2O_3/n-Al_2O_3(-)$ prepared using incipient wetness impregnation of a nitrate precursor, since this leads to the smallest Sm_2O_3 particles as well as the largest coverage of the acidic Al_2O_3 support. XRD analysis revealed that high-temperature calcinations form $SmAlO_3$ on the Al_2O_3 -supported catalysts. While this reduced the near surface Sm_2O_3 concentration, it had beneficial effects as it also lowered the Al_2O_3 content. Therefore, Al_2O_3 -supported Sm_2O_3 warrants further investigation, as surface modifications of the Al_2O_3 can reduce its acidity and lead to higher C_2 selectivities in the oxidative coupling of methane over these catalysts.

Published by Elsevier B.V.

1. Introduction

The conversion of ethylene to higher hydrocarbons is a frequently used industrial process, mainly for polymerization, oxidation, and halogenation reactions [1–3]. Currently, ethylene is synthesized using steam cracking of gaseous or light liquid hydrocarbons [4]. Given the abundance of natural gas, however, there is significant interest in using natural gas as the feedstock for the production of short hydrocarbons. Methane, the main component (>90%) of natural gas, is one possible raw material. One of the first oxidative coupling of methane (OCM) investigations occurred in the early 1980s [5] and it was discovered that methane (CH_4) and oxygen (O_2) fed over a catalyst at elevated temperatures produce the usual combustion products (CO_2 , CO , H_2O) along with ethane (C_2H_6), ethylene (C_2H_4), and hydrogen (H_2). The impediment for using OCM as an industrial process is the low reaction yield for ethane and ethylene (C_2 products). Generally, highly active catalysts for OCM have a C_2 selectivity less than 70% at a methane

conversion of ~20–30% with the maximum observed C_2 yield being in the 20% range [6–10]. The reason for the low C_2 yields can be attributed to the thermodynamics and kinetics of the OCM reaction. Both the complete oxidation and the partial oxidation of methane are exothermic reactions ($\Delta H^\circ = -890$ kJ/mol for complete oxidation vs. $\Delta H^\circ = -175$ kJ/mol for C_2H_6 formation, using standard heats of formation). As the complete oxidation yields products with a lower energy (CO_x) this is the thermodynamically favored reaction pathway. The activation energies for the formation of ethane ($E_a = 135$ kJ/mol) and ethylene ($E_a = 173$ kJ/mol) are considerably higher than the activation energy for the total combustion of methane and ethane ($E_a = 66$ kJ/mol and $E_a = 94$ kJ/mol, respectively) under the same conditions (700 °C and $CH_4:O_2 = 20:1$ using samaria as a catalyst [6]). Research has been focused on trying to increase the activity in the oxidative coupling of methane and decrease the oxidation rate to CO and CO_2 products.

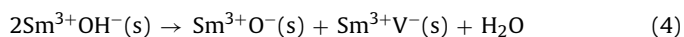
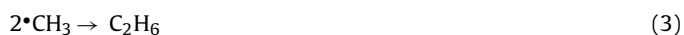
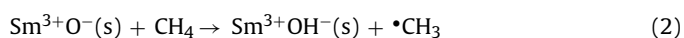
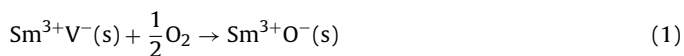
Several catalyst systems have been investigated in detail for their use in OCM. These include for example, alkali earth metal oxides catalysts [5,7,11–17], reducible non-transition metal oxides [8,18–22], and rare-earth oxides (REOs), especially samarium oxide (samaria) [2,9,10,23–33]. In particular, the lanthanides that form sesquioxides (Me_2O_3 , where Me is a metal ion) and do not form

* Corresponding author. Tel.: +1 352 392 6585; fax: +1 352 392 9513.

E-mail address: hweaver@che.ufl.edu (H.E. Hagelin-Weaver).

higher oxides (such as MeO_2) are successful in converting CH_4 to C_2 products. The high thermionic properties along with their natural basicity contribute to their ability to promote the partial oxidation pathway and therefore increase the C_2 product yield [17]. Conventional transition metal oxide and alkali metal oxide catalysts typically favor the combustion of both the methane feedstock and any formed C_2 products, and thus are not viable catalyst systems to study. In particular the irreducible rare earth oxides are active OCM catalysts, and the major factors playing a role in determining the C_2 selectivity for these REOs are the oxidation/reduction properties and the oxygen mobility [34].

Of all the lanthanides, samaria has been the most studied OCM catalyst, with the initial investigation performed by Otsuka [6]. This study showed that the C_2 rate of production for samaria was almost 3 times greater than the next best REO catalyst (lanthanum oxide) and these results were later confirmed in subsequent work [9]. Additionally, the reaction scheme for the catalytic surface interactions that occur during C_2H_6 production was formulated as shown in Eqs. (1)–(3). The active site(s) is(are) regenerated through water desorption from two neighboring $\text{Sm}^{3+}\text{OH}^-$ (Eq. (4)).



where V^- indicates a surface oxygen vacancy (or basic site). These sites, once occupied with a surface oxygen, are responsible for the hydrogen abstraction from the methane and form the surface hydroxide plus the $\bullet\text{CH}_3$ radical. Ethane is formed by the collision of the $\bullet\text{CH}_3$ radicals in the gas phase and the secondary product, ethylene, is produced by the dehydrogenation of ethane [24]. Zhang et al. discovered the role of O_2^- as the most probable active oxygen species for non-reducible REO based catalysts under OCM reaction conditions using Raman spectroscopy [10]. The supplementary in situ laser Raman spectroscopic study of the active-oxygen species for a different catalyst supported this claim [35,36].

In this study, we have investigated the effects of catalyst preparation method and the influence of various Al_2O_3 supports, on Sm_2O_3 nanoparticles and Al_2O_3 -supported Sm_2O_3 catalysts in the oxidative coupling of methane to obtain a better understanding of the factors influencing the catalytic activity and selectivity of Sm_2O_3 -based OCM catalysts. While more active multi-component catalysts have been reported in the literature, no additives or promoters were added in this study to investigate in detail the effects of the preparation method, the catalyst precursor and the Al_2O_3 support on the oxidative coupling of methane. Two Sm_2O_3 precursors (chloride and nitrate salts) were included in the study, and the Sm_2O_3 NP preparation methods investigated include thermal decomposition of a samarium-oleate complex and a water/toluene reverse microemulsion technique. The supported catalysts were prepared using incipient wetness impregnation of the oleate NPs or a samarium nitrate precursor, and samaria deposition using a modified reverse microemulsion technique onto three Al_2O_3 supports with varying properties, a high surface area nanoparticle alumina (n- $\text{Al}_2\text{O}_3(+)$) a low surface area nanoparticle alumina (n- $\text{Al}_2\text{O}_3(-)$), and a conventional γ - Al_2O_3 porous catalyst support (p- Al_2O_3). The effects of calcination temperature on the activity and selectivity of selected Sm_2O_3 NPs and $\text{Sm}_2\text{O}_3/\text{Al}_2\text{O}_3$ catalysts were also investigated. Each catalyst was tested at three different $\text{CH}_4:\text{O}_2$ ratios (9:1, 7:1, and 4:1) as well as two reaction temperatures (740 °C and 800 °C) using one fixed volumetric feed flow rate to observe trends in the activity and selectivity between catalysts and

reaction conditions. The catalysts were analyzed using BET surface area measurements, X-ray diffraction analysis and X-ray photoelectron spectroscopy to obtain their surface areas, crystal structures and surface compositions, and determine if and how these catalysts properties influence the catalytic activities and selectivities.

2. Experimental

2.1. Catalyst preparation

2.1.1. Samaria nanoparticle synthesis via metal-oleate decomposition

REO NPs were synthesized via decomposition of an REO oleate complex using a slightly modified literature procedure [37]. Briefly, 16 mmol of the REO precursor (samarium (III) nitrate or chloride, 99.9% REO, REacton, Alfa Aesar) and 48 mmol of sodium oleate (received from TCI) were mixed together in a two-phase solution consisting of 28 mL hexane (ACS grade, Fisher), 16 mL ethanol (histological grade, Fisher) and 12 mL deionized (DI) water. The mixture was stirred vigorously and was allowed to age at reflux (60 °C) for 4 h. After reaction, the resulting samarium-oleate complex is in the organic phase while the salts from the precursors are in the aqueous phase. The samarium-oleate complex was isolated from the aqueous phase by means of a separatory funnel and washed with DI water three times in order to remove any residual salts. Afterwards, the hexane was removed by a rotary evaporator. The complex was then mixed with 50 mL of tri-n-octylamine (TCI, 90%) and 8 mmol of oleic acid (Alfa Aesar, tech. grade, 90%) for the high temperature decomposition step. The heating program used for the decomposition is as follows:

1. Ramp to 100 °C at 8 °C/min.
2. Hold at 100 °C for 20 min (outgas step).
3. Ramp to 350 °C at 4 °C/min.
4. Hold at 350 °C for 3 h.

After the decomposition step, the NPs were recovered by destabilizing the suspension using ethanol. Sonication of the resulting mixture for 20 min was done to remove most of the capping agent remaining on the surface. The NPs were then collected by centrifugation followed by redispersing them in hexane. This process was repeated several times to maximize capping agent removal. The samaria NPs were calcined at 800 °C for 4 h unless otherwise stated and are labeled $\text{Sm}_2\text{O}_3(\text{Cl})\text{-OM}$ and $\text{Sm}_2\text{O}_3(\text{N})\text{-OM}$ according to Table 1.

2.1.2. Samaria nanoparticle synthesis via microemulsion method

Samaria NPs were also synthesis via a modified previously reported [38] reverse microemulsion method for comparison. Using this method, 22.5 mL of DI water with the dissolved samaria nitrate salt precursor (4.0 g) was mixed vigorously with 186 mL of toluene. The amount of precursor was the amount that would yield a 1.5-g batch of samarium oxide. The microemulsion surfactant, Tween 80, was then added dropwise under vigorous stirring until a microemulsion was formed (approximately 2–4 mL of Tween), afterwards an extra 1–2 mL was added in order to prevent the aqueous sodium hydroxide solution from breaking the microemulsion. 15 mL of an aqueous sodium hydroxide solution was then added dropwise to precipitate samarium hydroxide. 50% excess of the sodium hydroxide was used in order to maximize the yield of the samarium hydroxide. The microemulsion solution was allowed to stir vigorously overnight and was then centrifuged to separate the solid product from the liquid phase. The hydroxide NPs were then dispersed in 200 mL of an ethanol/water mixture (50%, v/v). The solution was sonicated for an hour and centrifuged again to collect

Table 1
BET surface areas obtained from the different Sm₂O₃ nanoparticles and Sm₂O₃/Al₂O₃ catalysts.

Catalyst description ^a	Sm ₂ O ₃ Prep. ^b	Catalyst Prep. ^c	SSA ^d [m ² /g]	Particle size from BET [nm]	Particle size from XRD [nm]
Nanoparticles					
Sm ₂ O ₃ (Cl)-OM	OM	–	8.5	85	25
Sm ₂ O ₃ (N)-OM	OM	–	14.5	50	14
Sm ₂ O ₃ (N)-ME	ME	–	4.5	160	43
Sm ₂ O ₃ (Cl)-OM ^h	OM	–	3.0	240	29
Sm ₂ O ₃ (N)-OM ^h	OM	–	1.1	650	20
Al₂O₃-Supported Sm₂O₃					
Sm ₂ O ₃ /p-Al ₂ O ₃ -OM	OM	IM	145		
Sm ₂ O ₃ /p-Al ₂ O ₃ -IM	–	IM	125		
Sm ₂ O ₃ /p-Al ₂ O ₃ -ME	–	ME	125		
Sm ₂ O ₃ /n-Al ₂ O ₃ (+)-OM	OM	IM	130		
Sm ₂ O ₃ /n-Al ₂ O ₃ (-)-OM	OM	IM	85		
Sm ₂ O ₃ /n-Al ₂ O ₃ (+)-IM	–	IM	80		
Sm ₂ O ₃ /n-Al ₂ O ₃ (-)-IM	–	IM	50		
Sm ₂ O ₃ /p-Al ₂ O ₃ -IM ^h	–	IM	43		
Sm ₂ O ₃ /p-Al ₂ O ₃ -ME ^h	–	ME	60		
Al₂O₃ Supports^e				NH₃ cm³/g^f	CO₂ cm³/g^g
n-Al ₂ O ₃ (+)	–	–	695	9.0	0.75
n-Al ₂ O ₃ (-)	–	–	275	8.3	0.6
p-Al ₂ O ₃	–	–	260	1.6	1.75

^a 100% Sm₂O₃ nanoparticles (NPs), or 20% Sm₂O₃ by weight on an Al₂O₃ support. (Cl): samarium chloride precursor used for nanoparticle (NP) preparation, and (N): samarium nitrate precursor used for nanoparticle or catalyst preparation.

^b Sm₂O₃ Prep.: OM = Sm₂O₃ NPs prepared using the oleate method. ME = Sm₂O₃ NPs prepared using reverse microemulsion method.

^c Catalysts prepared via the incipient wetness impregnation method (IM) using an aqueous solution of samarium nitrate (IM) or a hexane dispersion of OM nanoparticles (OM), or via a modified reverse microemulsion method (ME).

^d Specific Surface Area (SSA) as determined by BET analysis. After calcination treatment at 800 °C (or 1000 °C) for the Sm₂O₃ NPs and Sm₂O₃/Al₂O₃ catalysts, or after drying at 100 °C for the Al₂O₃ supports.

^e Al₂O₃ supports; Al₂O₃(+) and Al₂O₃(-) from NanoScale Inc. and γ -Al₂O₃ from Alfa Aesar.

^f NH₃ adsorption (standard cm³/g) to determine acidic sites.

^g CO₂ adsorption (standard cm³/g) to determine basic sites.

^h Catalysts calcined at 1000 °C before reaction instead of 800 °C

the final product. The NPs were dried overnight at 105 °C before calcination.

2.1.3. Preparation of Al₂O₃-supported Sm₂O₃

Three different types of supported Sm₂O₃ catalysts were prepared using two main methods of Sm₂O₃ deposition onto the support, namely, incipient wetness impregnation and a reverse microemulsion technique. Furthermore, three different alumina supports were used in the synthesis of the supported catalysts, the conventional p-Al₂O₃ catalyst support from Alfa Aesar, the high surface area n-Al₂O₃(+) from NanoActive, and the lower surface area n-Al₂O₃(-) also from NanoActive. In all cases, the samarium nitrate precursor was used to facilitate comparisons. Two sets of catalysts were prepared using incipient wetness impregnation (IWI) of either an aqueous solution of samarium nitrate or a hexane dispersion of the samaria NPs formed via the metal oleate methodology. The third type of catalyst was prepared using a reverse microemulsion technique to deposit the samaria onto the support.

For loading the samarium nitrate salt using the IWI method, the precursor was dissolved in a volume of DI water equal to that of the catalysts support pore volume, or the minimum amount of solvent which would completely dissolve the precursor, and was then mixed with the catalyst support until incipient wetness. The second IWI method used the samaria NPs prepared using the oleate method and the samarium nitrate precursor. As post-calcination NPs, with the capping agent removed, did not disperse in the solvent used, the recovered samaria NPs were dispersed in hexane before the calcination step. After each loading step the catalyst was dried to remove the hexane/water from the catalyst pores, and the loading step was repeated until the desired loading concentration was obtained (20% Sm₂O₃ by weight on the support). After the final impregnation step (usually the 2nd or 3rd impregnation), the catalysts were dried overnight at 105 °C and calcined at 800 °C for 4 h unless stated otherwise.

The third catalyst was prepared using a heterogeneous reverse microemulsion methodology which has been previously reported in the lab [39]. Modifications to the procedure were made in order to be consistent with the procedure for the pure samaria NP microemulsion experiments. Briefly, 3.4 g of p-Al₂O₃ support was suspended in 22.5 mL DI water prior to the addition of 2.2 g samarium nitrate salt. The resulting mixture was then added to 186 mL toluene under vigorous stirring. The addition of the surfactant and NaOH solution was the same as for the pure Sm₂O₃ microemulsion method. After collection, half of the catalyst was calcined at 800 °C while the other half was calcined at 1000 °C.

2.2. Characterization methods

Brunauer–Emmett–Teller (BET) surface area measurements for all catalysts were performed using a 6-point isotherm on a Quantachrome NOVA 1200 instrument operating at liquid nitrogen temperatures. Particle size calculation based on the BET surface areas are calculated using Eq. (5). The calculation is based on the assumption of having monodisperse, spherical particles.

$$d_p = \frac{6}{SA \cdot \rho_p} \quad (5)$$

where SA is the specific surface area [m²/g] and ρ_p [g/m³] is the particle density.

X-ray diffraction (XRD) patterns for select catalysts were collected on a Phillips APD 3720 Xray diffractometer using Cu K α radiation ($\lambda = 1.54 \text{ \AA}$). Catalyst powders were pressed onto double sided sticky tape and secured on a glass slide. An average crystallite size was calculated using the Scherrer equation (Eq. (6)).

$$d_p = \frac{K\lambda}{\beta \cos(\theta)} \quad (6)$$

In the Scherrer equation, d_p is the crystallite size (nm), K is the shape factor (taken as unity), λ is the Cu K α radiation wavelength (nm), β is the peak width at half the maximum intensity (FWHM) in radians, and θ is the Bragg angle, which is half of the diffraction angle (2θ).

TEM images were collected using a JEOL 2010F instrument using an accelerating voltage of 200 kV. Samples were dispersed in hexane and sonicated for 15 min before being loaded onto a 400 mesh copper grid with a carbon film. Several TEM images were recorded at various locations on the sample and at different magnifications to confirm that the structures observed were present throughout the catalyst. For each catalyst representative images are presented in the figures.

XPS measurements were performed on a PerkinElmer 5100 XPS system using an aluminum x-ray source. Samples were dried in an oven overnight at 105 °C to minimize the water adsorption on the catalyst surface. For survey scans the time/step was 30 ms with a 0.5 eV step size, and a pass energy of 89.45 eV. For high resolution (narrow) scans, the time/step was 50 ms, the step size 0.1 eV, and the pass energy 35.75 eV. Both survey and high-resolution spectra were collected using a total of 10 scans. Samples were prepared by placing a thin layer of catalyst on double-sided carbon conductive tape. Scan shifts were taken into account by referencing to the C 1s peak at 284.6 eV. The Si 2p peak at 99 eV, observed on all three catalysts, is due to the sample holder or the instrument rather than the sample. This was confirmed in a different XPS instrument which uses an aluminum cup as the sample holder (rather than the carbon conductive tape) and no Si peak was detected in the spectra obtained in this system.

2.3. OCM reaction experiments

Catalytic activity measurements were carried out in a quartz tube reactor with an inner diameter of 10 mm. The quartz tube reactor was used in a previously reported reactor system, which was slightly modified for the current application [40]. Each catalyst was pressed into a pellet, using a Carver pellet press, then crushed and sieved to a size range of 180–250 microns. For loading the reactor, 0.4 g of the sieved catalysts (either Sm₂O₃ NPs or Al₂O₃-supported Sm₂O₃) was supported in the quartz reactor tube between two pieces of quartz wool. CH₄, O₂, and an internal standard (N₂) were fed through the system at a rate of 120 standard cm³ per minute (sccm) (with N₂ constant at 23.2 sccm) using three mass flow controllers (MFCs). This results in a GHSV of 1760 h⁻¹ for the supported catalysts and 880 h⁻¹ for the pure samaria NPs. Three different CH₄:O₂ ratios (9:1, 7:1, and 4:1) at two temperature settings (740 and 800 °C) were used to observe the effects of the reaction parameters on the activity, selectivity and product distribution in the oxidative coupling of methane (OCM). Product analysis was performed on a custom-configured on-line Agilent 6890 N gas chromatograph (GC) equipped with both a thermal conductivity detector (TCD) and a flame ionization detector (FID) in series along with two packed columns, a polar Porapak Q capillary column and a molecular sieve, also in series with a column isolation valve in between the columns. The former was used to separate the CO₂, C₂H₆, and C₂H₄ and the latter for CH₄, O₂, N₂, CO, H₂ separation. Calibration curves for product formation and methane conversion were taken by feeding a known flow rate of the calibration gas and 23.2 sccm of internal standard (N₂) to the GC and measuring the calibration gas to N₂ TCD peak area ratio. All calibration curves were linear and regression analysis resulted in fit values of >99.3%. Measurements were taken at each reaction condition after 20 min to allow for the reaction to reach steady state and a repeat was taken to ensure reproducibility. The water produced during the reaction was separated from the gas phase products prior to entering the GC using a condenser trap emerged in an

ice-water bath. In addition to the CH₄ conversions (X_{CH_4}) defined as the methane reacted over the total amount of methane fed to the reactor (Eq. (7)), a CH₄ conversion to C₂ and CO_x products ($X_{\text{CH}_4}^*$) was defined and calculated according to Eq. (8). This was done to obtain an estimate of the coking in the reactions. The C₂ selectivity was defined as the methane reacted to form C₂ products over the methane reacted to C₂ plus CO_x products (Eq. (9)) and is reported as a percentage. C₂ product yield (Eq. (10)) was calculated as the methane conversion ($X_{\text{CH}_4}^*$) (according to Eq. (8)) multiplied by the selectivity (Eq. (9)). Repeat reaction experiments involving reloading the catalyst resulted in standard deviations of 0.5% for both the CH₄ conversion and the C₂ selectivity.

$$X_{\text{CH}_4} = \frac{\text{CH}_{4,\text{in}} - \text{CH}_{4,\text{out}}}{\text{CH}_{4,\text{in}}} \quad (7)$$

$$X_{\text{CH}_4}^* = \frac{[2 \cdot (\text{C}_2\text{H}_6 + \text{C}_2\text{H}_4) + \text{CO} + \text{CO}_2]_{\text{out}}}{\text{CH}_{4,\text{in}}} \quad (8)$$

$$S_{\text{C}_2} = \frac{\text{sccm C}_2\text{products}}{\text{sccm CH}_4\text{ reacted to C}_2\text{ and CO}_x} \quad (9)$$

$$\text{C}_2 \text{ Yield [\%]} = X_{\text{CH}_4}^* \cdot S_{\text{C}_2} \cdot 100 \quad (10)$$

3. Results and discussion

The prepared Sm₂O₃ catalysts were subjected to methane coupling experiments and catalyst characterizations.

3.1. OCM activity measurements

The catalytic activity and selectivity of all catalysts in the oxidative coupling of methane to C₂ hydrocarbons were evaluated at the two different temperatures, 740 °C and 800 °C. The results are presented in Tables 2 and 3 and Figs. 1–5.

3.1.1. Pure samaria nanoparticles

The samaria NPs were synthesized via the oleate-method using chloride and nitrate salt precursors and via the reverse microemulsion using the nitrate salt to determine the effects of samaria precursor and preparation method on the Sm₂O₃ particle size and how these parameters affect the OCM activity and selectivity. Fig. 1A and B display the OCM reaction data for the pure samaria NPs from the oleate and microemulsion methods at reaction temperatures of 740 °C and 800 °C, respectively. The results are also summarized in Tables 2 and 3. A few general trends, which are the same for most catalysts, can be observed from the reaction results (Fig. 1A and B plus Tables 2 and 3). In most cases, the methane conversion increases and the selectivity decreases as the CH₄:O₂ ratio decreases from 9:1 to 4:1, i.e. more CH₄ reacts but a larger fraction is converted to CO and CO₂ at the higher O₂ concentrations. This is to be expected and is the reason why CH₄ concentrations significantly higher than the stoichiometric CH₄:O₂ ratio for ethane or ethylene formation is often used in this reaction [17]. However, since the decrease in selectivity is smaller than the increase in conversion with decreasing CH₄:O₂ ratio, the highest C₂ yields are obtained at the 4:1 CH₄:O₂ ratio for most Sm₂O₃ NP catalysts (Table 2). As can be seen in Table 2, most of the methane reacted over the Sm₂O₃ nanoparticles forms C₂ or CO_x products. The largest differences between X_{CH_4} and $X_{\text{CH}_4}^*$ are observed at a CH₄:O₂ ratio of 4:1, which at first appears unusual as coking would not be expected at the highest O₂ concentrations. However, the C₂ yield is higher at the lower CH₄:O₂ ratios, which can increase coke formation as the C₂ products decompose easier than CH₄. Furthermore, coking is more likely at higher temperatures, and the increased conversion, in particular to CO_x, will result in more heat released from the exothermic reactions. This is evident as a larger difference between

Table 2
Oxidative coupling of methane over all catalysts at 740 °C and 800 °C.

Catalyst ^a	CH ₄ :O ₂ ratio	T = 740 °C				T = 800 °C			
		X _{CH₄} [%]	X* _{CH₄} [%]	S _{C₂} [%]	Y _{C₂} [%]	X _{CH₄} [%]	X* _{CH₄} [%]	S _{C₂} [%]	Y _{C₂} [%]
Sm₂O₃ nanoparticles									
Sm ₂ O ₃ (Cl)-OM	9	7.5	7.5	44.0	3.4	8.5	8.5	51.0	4.4
	7	10.5	10.5	44.0	4.6	12.5	12.5	47.0	6.0
	4	18.5	17.5	43.5	7.6	19.0	17.5	41.0	7.2
Sm ₂ O ₃ (N)-OM	9	10.0	10.0	58.5	6.0	10.0	10.0	57.0	5.8
	7	12.5	12.0	55.5	6.7	12.0	11.5	53.5	6.2
	4	19.5	18.0	43.5	7.8	19.0	17.0	40.0	6.8
Sm ₂ O ₃ (N)-ME	9	10.5	10.0	50.5	5.1	8.5	8.5	37.5	3.2
	7	13.0	12.0	52.5	6.3	13.0	11.0	47.5	5.2
	4	17.5	16.0	30.0	4.8	18.0	15.5	28.0	4.3
Sm₂O₃/Al₂O₃ catalysts									
Sm ₂ O ₃ /p-Al ₂ O ₃ -OM	9	6.0	5.0	6.0	0.3	6.5	6.0	18.0	1.1
	7	7.5	7.0	7.5	0.5	8.5	7.5	20.0	1.5
	4	15.0	12.5	10.5	1.3	19.0	14.5	24.5	3.6
Sm ₂ O ₃ /p-Al ₂ O ₃ -ME	9	6.0	6.0	22.0	1.3	7.5	7.5	34.0	2.6
	7	8.5	8.5	20.5	1.7	10.0	9.0	30.0	2.7
	4	16.5	14.0	21.0	2.9	18.5	15.0	28.0	4.2
Sm ₂ O ₃ /p-Al ₂ O ₃ -IM	9	8.5	7.0	19.5	1.4	9.0	7.5	28.5	2.1
	7	10.5	8.5	19.0	1.6	12.0	9.5	28.5	2.7
	4	20.5	15.5	24.5	3.8	21.5	16.5	27.5	4.5
p-Al ₂ O ₃	4	16.0	10.5	8.5	0.9	–	–	–	–
n-Al ₂ O ₃ (–)	4	14.0	11.5	10.0	1.1	–	–	–	–
Sm ₂ O ₃ /n-Al ₂ O ₃ (+)-OM	4	14.5	12.0	15.0	1.8	18.5	13.5	21.0	2.8
Sm ₂ O ₃ /n-Al ₂ O ₃ (+)-IM	4	18.5	14.0	17.5	2.5	20.5	15.5	24.5	3.8
Sm ₂ O ₃ /n-Al ₂ O ₃ (–)-OM	4	16.5	14.5	23.5	3.4	17.0	14.5	23.5	3.4
Sm ₂ O ₃ /n-Al ₂ O ₃ (–)-IM	4	19.5	16.0	32.0	5.1	20.0	16.0	35.0	5.6
Sm ₂ O ₃ /p-Al ₂ O ₃ -ME ^b	4	18.5	16.0	31.0	5.0	19.5	16.0	30.5	4.9
Sm ₂ O ₃ /p-Al ₂ O ₃ -IM ^b	4	19.0	15.0	24.0	3.6	21.5	15.5	27.5	4.3

^a Catalyst descriptions are given in Table 1. X_{CH₄}: methane conversion [%], X*_{CH₄}: methane conversion to C₂ and CO_x products [%], S_{C₂}: selectivity, i.e. methane reacted to C₂ products over methane reacted to C₂ and CO_x products [%], Y_{C₂}: C₂ yield (X*_{CH₄} · S_{C₂}) [%]

^b Catalysts calcined at 1000 °C before reaction instead of 800 °C.

Table 3
Product distribution data for the oxidative coupling of methane over all catalysts at 740 °C and 800 °C.

Catalyst ^a	CH ₄ :O ₂ ratio	Product distribution [%] at 740 °C				Product distribution [%] at 800 °C			
		C ₂ H ₄	C ₂ H ₆	CO ₂	CO	C ₂ H ₄	C ₂ H ₆	CO ₂	CO
Sm₂O₃ nanoparticles									
Sm ₂ O ₃ (Cl)-OM	9	17.4	26.6	44.7	11.3	29.7	21.4	40.3	8.6
	7	19.3	24.7	46.4	9.7	29.8	17.3	44.9	8.0
	4	22.7	20.6	50.3	6.5	28.3	12.9	51.1	7.7
Sm ₂ O ₃ (N)-OM	9	25.5	33.2	35.8	5.5	36.0	21.0	34.8	8.2
	7	25.4	30.0	38.6	6.0	34.7	18.9	38.0	8.4
	4	22.9	20.7	49.2	7.2	27.6	12.3	50.4	9.7
Sm ₂ O ₃ (N)-ME	9	23.0	27.6	41.8	7.6	21.5	16.0	49.5	13.0
	7	23.9	28.7	39.4	8.0	29.4	18.3	42.4	10.0
	4	15.3	14.5	60.3	10.0	19.2	8.7	59.5	12.6
Sm₂O₃/Al₂O₃ catalysts									
Sm ₂ O ₃ /p-Al ₂ O ₃ -OM	9	0.8	5.4	62.1	31.7	8.7	9.4	47.5	34.4
	7	1.5	5.8	61.4	31.3	11.0	8.7	47.5	32.7
	4	4.5	6.1	59.7	29.7	18.3	6.3	43.7	31.7
Sm ₂ O ₃ /p-Al ₂ O ₃ -ME	9	5.8	15.9	55.4	22.9	19.8	14.3	46.5	19.4
	7	5.8	14.5	57.5	22.2	16.4	13.5	50.1	19.9
	4	9.2	11.8	60.7	18.3	19.3	8.8	53.4	18.6
Sm ₂ O ₃ /p-Al ₂ O ₃ -IM	9	7.1	12.4	51.5	29.0	15.9	12.4	43.8	27.9
	7	6.5	12.5	52.5	28.5	17.8	10.9	45.2	26.1
	4	13.7	10.8	53.5	22.0	20.1	7.6	50.0	22.4
p-Al ₂ O ₃	4	2.4	6.1	52.8	38.6	–	–	–	–
n-Al ₂ O ₃ (–)	4	1.7	8.5	78.6	11.2	–	–	–	–
Sm ₂ O ₃ /n-Al ₂ O ₃ (+)-OM	4	7.8	7.0	62.2	23.0	14.8	6.4	49.4	29.5
Sm ₂ O ₃ /n-Al ₂ O ₃ (–)-OM	4	13.2	10.4	59.5	16.9	15.2	8.2	59.6	17.1
Sm ₂ O ₃ /n-Al ₂ O ₃ (+)-IM	4	8.4	9.0	54.7	28.0	17.2	7.3	49.1	26.4
Sm ₂ O ₃ /n-Al ₂ O ₃ (–)-IM	4	17.4	14.7	49.9	18.0	24.1	10.9	48.5	16.5
Sm ₂ O ₃ /p-Al ₂ O ₃ -ME ^b	4	17.0	14.0	55.4	13.6	21.5	9.0	52.3	17.2
Sm ₂ O ₃ /p-Al ₂ O ₃ -IM ^b	4	12.0	12.2	53.6	22.2	19.8	7.7	44.9	27.6

^a Catalyst descriptions are given in Table 1.

^b Catalysts calcined at 1000 °C before reaction instead of 800 °C.

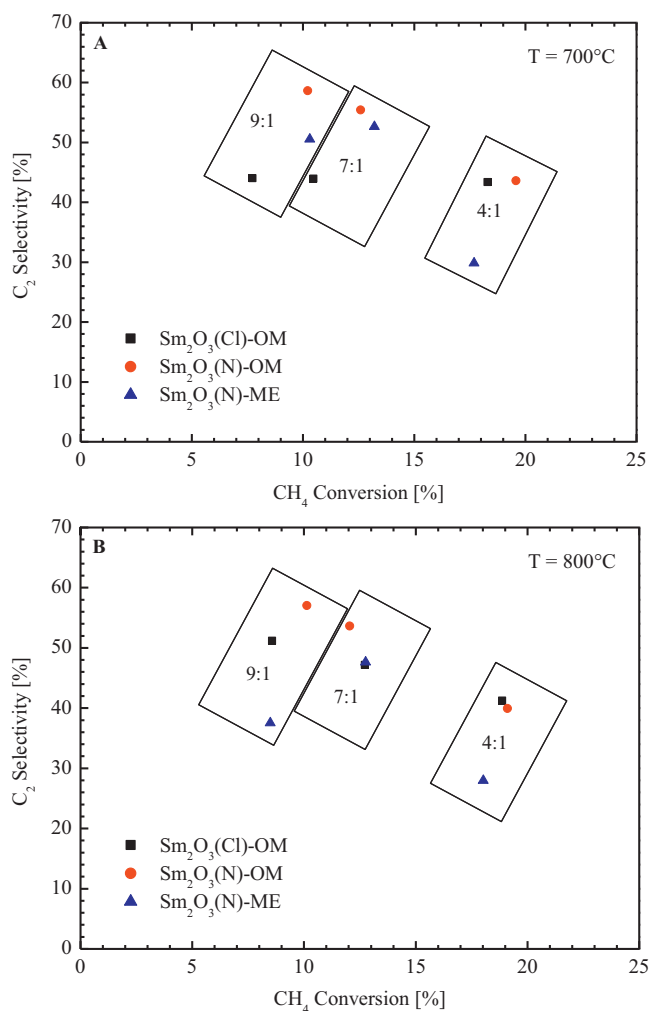


Fig. 1. OCM reaction data for Sm_2O_3 nanoparticles prepared using the oleate decomposition with nitrate and chloride precursors and the reverse microemulsion method using a samarium nitrate precursor. The numbers in the boxes indicate the $\text{CH}_4:\text{O}_2$ feed ratios, i.e. 4:1, 7:1 and 9:1. (A) reaction temperature of 740 °C and (B) reaction temperature of 800 °C.

the X_{CH_4} and $X_{\text{C}_2\text{H}_4}^*$ at 800 °C versus 740 °C (Table 2). Coking for all Sm_2O_3 NP catalysts was observed on the reactor walls downstream of the catalyst bed and not on the Sm_2O_3 NPs. This is in an oxygen-deficient region of the reactor, as the O_2 conversion in all cases is at least close to 100%, and indicates that coking over the Sm_2O_3 is negligible.

The $\text{CH}_4:\text{O}_2$ ratio also affects the product distribution as can be seen in Table 3. As expected, the CO_2 content in the product stream increases with increasing O_2 concentration. The change in CO concentration with $\text{CH}_4:\text{O}_2$ ratio is not as significant, and the trend depends on the specific Sm_2O_3 NPs. The CO concentration increases slightly over the $\text{Sm}_2\text{O}_3(\text{N})\text{-OM}$ and $\text{Sm}_2\text{O}_3(\text{N})\text{-ME}$ catalysts, while it decreases with increasing O_2 concentration over the $\text{Sm}_2\text{O}_3(\text{Cl})\text{-OM}$ catalyst. Therefore, the $\text{CO}_2\text{-to-CO}$ product ratio nearly doubles over the $\text{Sm}_2\text{O}_3(\text{Cl})\text{-OM}$ catalyst, while there is only a slight increase (if any) in this ratio with decreasing $\text{CH}_4:\text{O}_2$ ratio for the $\text{Sm}_2\text{O}_3(\text{N})\text{-OM}$ and $\text{Sm}_2\text{O}_3(\text{N})\text{-ME}$ catalysts. At 740 °C and the higher $\text{CH}_4:\text{O}_2$ ratios (9:1 and 7:1) the $\text{C}_2\text{H}_4:\text{C}_2\text{H}_6$ product ratio is below one, i.e. more C_2H_6 than C_2H_4 is formed, while at the highest O_2 concentration ($\text{CH}_4:\text{O}_2$ ratio = 4:1) more C_2H_4 is formed than C_2H_6 over all Sm_2O_3 NP catalysts. This is consistent with the trend expected from the stoichiometry, i.e. more oxygen (lower $\text{CH}_4:\text{O}_2$ ratio) is required for production of C_2H_4 versus C_2H_6 (Eqs. (11)

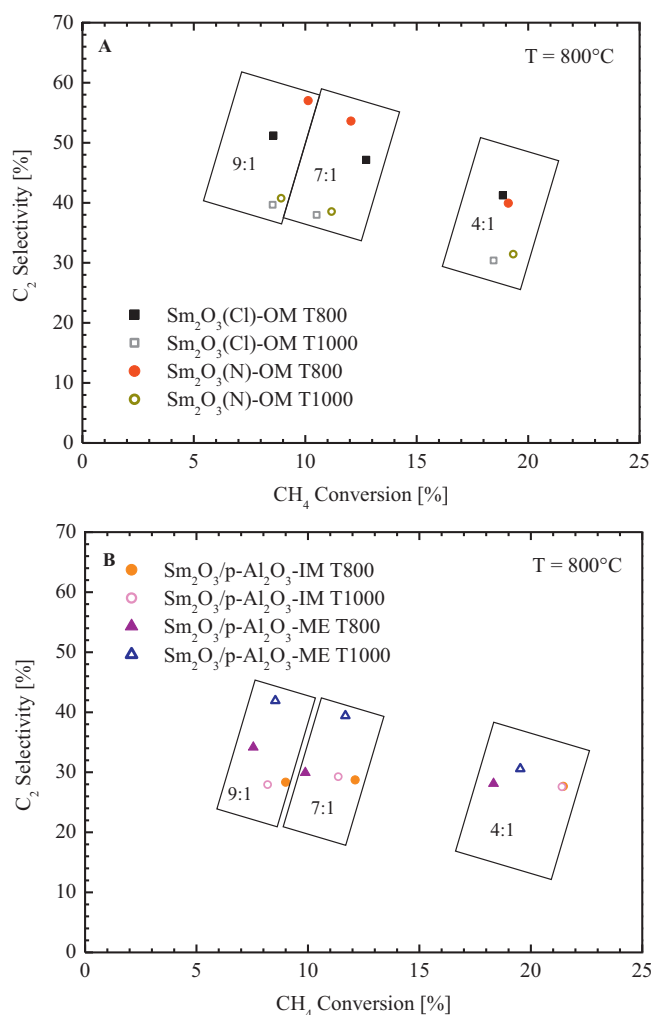


Fig. 2. Effects of calcination temperature between 800 °C and 1000 °C in the OCM reaction data for (A) Sm_2O_3 nanoparticles prepared using the oleate decomposition method with nitrate and chloride precursors and (B) $\text{Sm}_2\text{O}_3/\text{p-Al}_2\text{O}_3$ catalysts prepared using incipient wetness impregnation with an aqueous solution of samarium nitrate and the reverse microemulsion method. The data was collected at a reaction temperature of 800 °C and at different $\text{CH}_4:\text{O}_2$ feed ratios, i.e. 4:1, 7:1 and 9:1 (as indicated by the numbers inside the boxes).

and (12)). It is interesting to note that at each $\text{CH}_4:\text{O}_2$ ratio the $\text{C}_2\text{H}_4:\text{C}_2\text{H}_6$ product ratio is the same for the Sm_2O_3 NPs regardless of preparation method and precursor, and this ratio increases from 0.8 to 1.1 as the $\text{CH}_4:\text{O}_2$ ratio is decreased from 9:1 to 4:1. This suggests that the formation of the secondary C_2H_4 product is not dependent on the Sm_2O_3 surface over these NPs. This observation is supported by an earlier OCM study over 1% $\text{Sr}/\text{La}_2\text{O}_3$ [24].



The effects of reaction temperature are different dependent on whether a chloride or nitrate precursor was used in the preparation of the Sm_2O_3 NPs. While the CH_4 conversion is not altered significantly, the C_2 selectivity decrease with increasing reaction temperature (between 740 °C and 800 °C) for the Sm_2O_3 NPs prepared using nitrate precursors, irrespective of preparation method (oleate method or reverse microemulsion). The C_2 yields are therefore lower at 800 °C versus 740 °C (Table 2). In contrast, the CH_4 conversion and the C_2 selectivity both increase with increasing reaction temperature for the $\text{Sm}_2\text{O}_3(\text{Cl})\text{-OM}$ nanoparticles, for all except the 4:1 $\text{CH}_4:\text{O}_2$ ratio (which exhibit a slight decrease in C_2

selectivity). However, the C_2 yields for the $Sm_2O_3(Cl)$ -OM NPs at $800^\circ C$ are still lower than for the $Sm_2O_3(N)$ -OM NPs at $740^\circ C$.

The $C_2H_4:C_2H_6$ product ratio is significantly higher at $800^\circ C$ than at $740^\circ C$. In fact, at a reaction temperature of $800^\circ C$ more C_2H_4 than C_2H_6 product is formed at all $CH_4:O_2$ ratios over all Sm_2O_3 NPs. Over the $Sm_2O_3(N)$ -OM NP catalyst, the CO_2 content in the product stream is similar at both $740^\circ C$ and $800^\circ C$, but the CO content is higher at $800^\circ C$, and a higher CO content at the higher reaction temperature is observed also over the $Sm_2O_3(N)$ -ME NP catalyst. This is expected since more CO would have enough energy to desorb from the catalyst surface before undergoing oxidation at the higher temperature. At $740^\circ C$ the CO is more strongly bound to the surface, and has a higher probability of being oxidized to CO_2 before desorbing. The lower C_2 selectivities at $800^\circ C$ thus appear to be mainly due to a higher CO formation rate for these catalysts.

From the reaction data, it is evident that the samaria NPs prepared using the oleate method with the nitrate precursor outperform both the $Sm_2O_3(Cl)$ -OM and the $Sm_2O_3(N)$ -ME nanoparticles, since the $Sm_2O_3(N)$ -OM catalyst at most conditions exhibits both the highest CH_4 conversion and the highest C_2 selectivity (Fig. 1A and B). This is true for all $CH_4:O_2$ ratios at $740^\circ C$ and most $CH_4:O_2$ ratios at $800^\circ C$ (Table 2). Only at $800^\circ C$ and a $CH_4:O_2$ ratio of 4:1 does the $Sm_2O_3(Cl)$ -OM give a higher C_2 yield than the $Sm_2O_3(N)$ -OM catalyst (although the $Sm_2O_3(Cl)$ -OM yield at $800^\circ C$ (7.2%) is not higher than the C_2 yield obtained over the $Sm_2O_3(N)$ -OM catalyst at $740^\circ C$ (7.8%). While a yield of 8% is not the highest reported in the literature, it is in line with the yields obtained over pure Sm_2O_3 [9]. Higher yields can be obtained at even lower $CH_4:O_2$ ratios, such as a 12% yield at a $CH_4:O_2$ ratio of 2.5 [28], but ratios below $CH_4:O_2 = 4:1$ were avoided in the current investigation for safety reasons, i.e. to make sure that the feed stream had methane concentrations above the upper flammability limit.

The effects of calcining the nanoparticles at $1000^\circ C$ instead of $800^\circ C$ were also investigated for the Sm_2O_3 NPs prepared using the oleate method. The higher calcination temperature results in a significant decrease in C_2 selectivity, and in most cases also a decrease in CH_4 conversion as illustrated in Fig. 2A. After calcination at $1000^\circ C$ the performance of the $Sm_2O_3(Cl)$ -OM and $Sm_2O_3(N)$ -OM NPs are similar, but in most cases this is inferior to the performance of the catalysts calcined at $800^\circ C$. Only at a reaction temperature of $740^\circ C$ and a $CH_4:O_2$ ratio of 9:1 is there an advantage to calcining the $Sm_2O_3(Cl)$ NPs at a higher temperature (not shown), as the CH_4 conversion increased from the 7.5% of the $800^\circ C$ calcination value to 9.5% ($1000^\circ C$ calcination) and the C_2 selectivity is similar (44% vs. 45.5%).

Therefore, calcination at a higher temperature is undesirable as it decreases the C_2 selectivity and thus also the C_2 yield in most cases. Only in cases where chlorines may be present on the surface could a higher calcination temperature improve the C_2 yield, but then only in very special circumstances. Avoiding chloride precursors in catalyst preparation is likely a more effective way to obtain a higher yield.

3.1.2. Supported Sm_2O_3 catalysts – effects of preparation methods

Three types of alumina-supported samaria catalysts were prepared to investigate the effects of samaria deposition method on the catalytic activity and selectivity of Al_2O_3 -supported Sm_2O_3 in the methane coupling reaction. A porous alumina was selected for this study as this is a typical alumina-based catalyst support. As described in the catalyst preparation section, the samaria was deposited using either an incipient wetness impregnation method or a modified reverse microemulsion method. For the IW method samarium nitrate dissolved in deionized water, or $Sm_2O_3(N)$ -OM nanoparticles dispersed in hexane, was used during the impregnation of the $p-Al_2O_3$ support. The reaction results obtained from

these catalysts are presented in Fig. 3A and B and have been included in Tables 2 and 3.

Compared to the unsupported Sm_2O_3 NP results, the performance of the alumina-supported Sm_2O_3 is inferior. Not only are the C_2 selectivities significantly lower at all temperatures and $CH_4:O_2$ ratios, the CH_4 conversions are also slightly lower for most $Sm_2O_3/p-Al_2O_3$ catalysts. A lower conversion is expected, since the amount of Sm_2O_3 in the reactor for the alumina-supported catalysts is only 20% of the amount used for the pure NP Sm_2O_3 reactions. The acidic alumina support is also expected to yield a much lower C_2 selectivity than that observed for pure Sm_2O_3 [41]. Moreover, compared to the Sm_2O_3 NP catalysts, the $X_{CH_4}^*/X_{CH_4}$ is lower on the Al_2O_3 -supported catalysts, particularly at the 4:1 $CH_4:O_2$ ratio. This means that slightly more coking takes place over the Al_2O_3 -containing catalysts and this was also observed as a change in color of the catalysts from white to black, as well as a small amount of black deposits on the reactor walls downstream of the catalyst bed. Despite the presence of coking, no decrease in CH_4 conversion as a function of time was observed during the experiments, which indicates that the amount of coking was not sufficient to block the active surface sites. This is consistent with coking mainly occurring on the Al_2O_3 support, and not on the Sm_2O_3 (as inferred from the Sm_2O_3 NP experiments, where no coking was observed on the Sm_2O_3). While coking did not result in deactivation with time on stream, coking should be minimized as it reduces the yield to desired products and at longer time-on-stream a decrease in activity is likely due to reactor blockage. Even though the Al_2O_3 -supported Sm_2O_3 catalysts exhibited lower CH_4 conversions and C_2 selectivities, the C_2 yield per gram of samarium is significantly higher over the $Sm_2O_3/p-Al_2O_3$ -ME and $Sm_2O_3/p-Al_2O_3$ -IM catalysts compared with the Sm_2O_3 NP catalysts. This is particularly true at the 4:1 $CH_4:O_2$ ratio.

Some of the trends in activity and selectivity with $CH_4:O_2$ ratio and reaction temperature are different for the alumina-supported Sm_2O_3 catalysts compared with the unsupported Sm_2O_3 NPs. While the CH_4 conversion increases with decreasing $CH_4:O_2$ ratio, just as for the unsupported Sm_2O_3 NPs, the C_2 selectivity either increases or is not changed significantly with decreasing $CH_4:O_2$ ratio over the alumina-supported Sm_2O_3 . This trend in selectivity is in contrast to what is normally observed over OCM catalysts, and may be due to different contributions from Sm_2O_3 and Al_2O_3 at the various $CH_4:O_2$ ratios. The effect of reaction temperature is also different between the unsupported and supported Sm_2O_3 catalysts. Increasing the reaction temperature from $740^\circ C$ to $800^\circ C$ increases both the CH_4 conversion and C_2 selectivity over the $Sm_2O_3/p-Al_2O_3$ catalysts. Therefore, while the unsupported Sm_2O_3 NP catalysts are superior at a reaction temperature of $740^\circ C$ and higher $CH_4:O_2$ ratios (9:1 and 7:1), at $800^\circ C$ and a $CH_4:O_2$ ratio of 4:1 the $Sm_2O_3/p-Al_2O_3$ catalysts can outperform the $Sm_2O_3(N)$ -ME NP catalyst and compete with the other Sm_2O_3 NP catalysts.

Evidently, the performance of the $Sm_2O_3/p-Al_2O_3$ catalysts is dependent on the preparation method. The worst performing catalyst is the $Sm_2O_3/p-Al_2O_3$ -OM catalyst, where the preformed Sm_2O_3 nanoparticles, prepared using the oleate method, are deposited onto the $p-Al_2O_3$ support using incipient wetness impregnation. Both the activity and the selectivity are lower on the $Sm_2O_3/p-Al_2O_3$ -OM catalyst, although the main reason for the inferior performance is the significantly lower C_2 selectivity compared to the other $Sm_2O_3/p-Al_2O_3$ catalysts. Of the three catalysts, the $Sm_2O_3/p-Al_2O_3$ prepared using the incipient wetness impregnation of an aqueous samarium nitrate solution ($Sm_2O_3/p-Al_2O_3$ -IM) has the best performance, since the CH_4 conversion is higher and the C_2 selectivity is either similar to or higher than those obtained over the $Sm_2O_3/p-Al_2O_3$ -OM and $Sm_2O_3/p-Al_2O_3$ -ME catalysts.

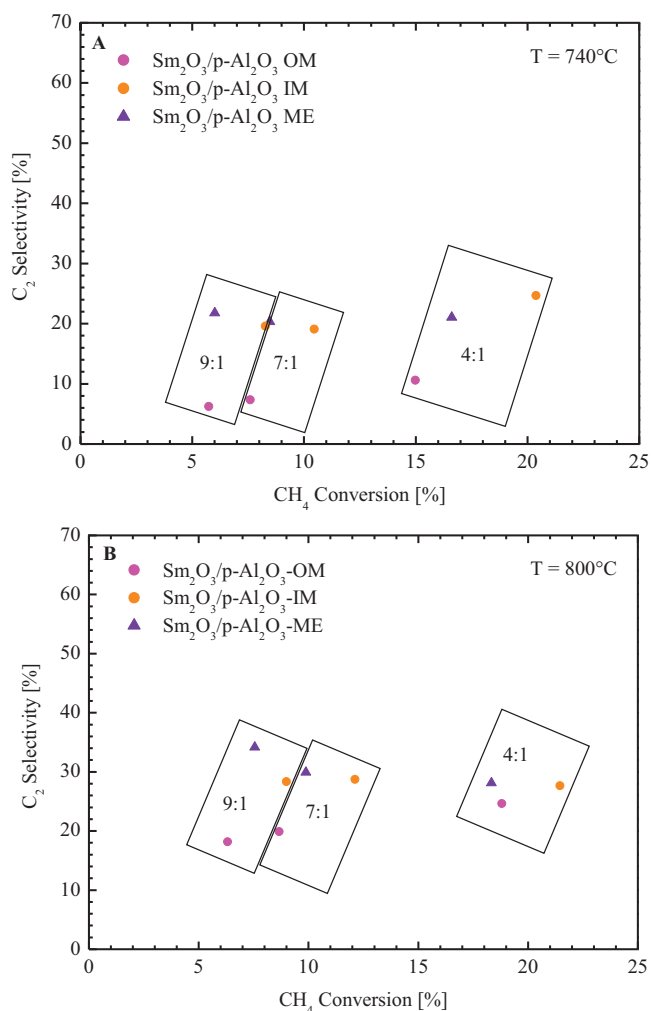


Fig. 3. OCM reaction data for Sm_2O_3 supported on $\text{p-Al}_2\text{O}_3$ prepared using incipient wetness impregnation of samarium nitrate (aqueous solution, IM) and a hexane dispersion of $\text{Sm}_2\text{O}_3(\text{N})$ -OM nanoparticles (OM) as well as a modified microemulsion method (ME). The numbers in the boxes indicate the $\text{CH}_4:\text{O}_2$ feed ratios, i.e. 4:1, 7:1 and 9:1. (A) reaction temperature of 740°C and (B) reaction temperature of 800°C .

Compared to the Sm_2O_3 NPs, the $\text{CO}_2:\text{CO}$ product ratios are lower over the $\text{Sm}_2\text{O}_3/\text{p-Al}_2\text{O}_3$ catalysts, as significantly more CO is formed over the supported catalysts. In most cases, the $\text{C}_2\text{H}_4:\text{C}_2\text{H}_6$ ratio is also lower for the supported catalysts. Only at a $\text{CH}_4:\text{O}_2$ ratio of 4:1 is the $\text{C}_2\text{H}_4:\text{C}_2\text{H}_6$ ratio higher for the $\text{Sm}_2\text{O}_3/\text{p-Al}_2\text{O}_3$ -IM catalyst compared with the unsupported catalysts. This is also true for the $\text{Sm}_2\text{O}_3/\text{p-Al}_2\text{O}_3$ -OM catalyst but only at a reaction temperature of 800°C . Clearly, the presence of an Al_2O_3 support alters the product distribution and results in lower C_2 yields, but the difference in C_2 yields is not as large as may be expected from an acidic support, and, moreover, the yield per gram of Sm_2O_3 is higher for the $\text{Sm}_2\text{O}_3/\text{p-Al}_2\text{O}_3$ catalysts compared with the Sm_2O_3 NPs. This indicates that Al_2O_3 may be considered as a support in OCM reactions, and it is possible that if the Al_2O_3 is doped to reduce the acidity of the surface, Al_2O_3 -supported Sm_2O_3 could be a competitive catalyst.

3.1.3. Supported Sm_2O_3 catalysts – effects of alumina support

Three different alumina supports, $\text{p-Al}_2\text{O}_3$, $\text{n-Al}_2\text{O}_3(+)$, and $\text{n-Al}_2\text{O}_3(-)$, were selected and loaded with 20% samaria by weight to determine the effects of alumina properties on $\text{Sm}_2\text{O}_3/\text{Al}_2\text{O}_3$ catalysts. These supports were chosen to probe the effects of support surface areas and varying acidic and basic support properties. As can be seen in Table 1, both the nanoparticle alumina supports

are very acidic (NH_3 adsorption = 8–9 standard cm^3/g) and have very few basic sites (CO_2 adsorption = 0.6–0.75 standard cm^3/g). In contrast, the $\text{p-Al}_2\text{O}_3$ support has significantly less acidic sites and an almost equal number of acidic and basic sites: 1.6 sccm/g NH_3 adsorption and 1.75 sccm/g CO_2 adsorption, respectively. Furthermore, the $\text{p-Al}_2\text{O}_3$ and $\text{n-Al}_2\text{O}_3(-)$ supports have similar surface areas (260–275 m^2/g), while the $\text{n-Al}_2\text{O}_3(+)$ has a significantly higher surface area (695 m^2/g).

To facilitate interpretation of the reaction data obtained from the $\text{Sm}_2\text{O}_3/\text{Al}_2\text{O}_3$ catalysts, two alumina supports, the $\text{p-Al}_2\text{O}_3$ and $\text{n-Al}_2\text{O}_3(-)$ calcined at 800°C , were subjected to the reaction conditions to determine any activity originating from the support. As can be seen in Table 2, the Al_2O_3 supports do exhibit some activity. At 740°C and a $\text{CH}_4:\text{O}_2$ ratio of 4:1 the CH_4 conversion over the $\text{p-Al}_2\text{O}_3$ support is similar to that obtained over the $\text{Sm}_2\text{O}_3/\text{p-Al}_2\text{O}_3$ -OM and $\text{Sm}_2\text{O}_3/\text{p-Al}_2\text{O}_3$ -ME catalysts under the same conditions. However, the conversion to C_2 and CO_x products (i.e. the $X_{\text{CH}_4}^*$) is lower, indicating that coking occurs over the bare supports. This is evident in the color change from white to black after reaction. Also, most of the CH_4 reacted over the support is converted to CO_2 or CO . The selectivity to C_2 products is only 8.5% over the $\text{p-Al}_2\text{O}_3$ support.

The $\text{n-Al}_2\text{O}_3(-)$ support exhibits a slightly different behavior compared with the $\text{p-Al}_2\text{O}_3$ support. The CH_4 conversion is somewhat lower, but the CH_4 conversion to C_2 and CO_x products is higher, i.e. there is less coking. The latter is clearly evident as this support is gray rather than black after reaction. The C_2 selectivity is also higher and so is the CO_2/CO ratio while the $\text{C}_2\text{H}_4/\text{C}_2\text{H}_6$ product ratio is lower.

The reaction data obtained from Sm_2O_3 deposited onto the different Al_2O_3 supports using the incipient wetness impregnation method of both the aqueous samarium nitrate solution and the hexane dispersion of Sm_2O_3 -OM NPs are presented in Figs. 4 and 5. As the trends observed on the $\text{Sm}_2\text{O}_3/\text{p-Al}_2\text{O}_3$ catalysts, i.e. the CH_4 conversion and C_2 selectivity increases with increasing temperature and decreasing $\text{CH}_4:\text{O}_2$ ratio, are the same for all alumina-supported catalysts, irrespective of catalyst preparation method and specific alumina support, only results obtained at the 4:1 $\text{CH}_4:\text{O}_2$ ratio are presented in Tables 2 and 3 (i.e. the feed ratio which gives the highest CH_4 conversion and C_2 selectivity). Despite the differences in specific surface areas as well as acid and basic properties, the CH_4 conversion does not vary significantly between the various Al_2O_3 supports. For most conditions, the variations in CH_4 conversion between catalysts prepared using the different Al_2O_3 supports is close to $\pm 1\%$. Thus, the method of Sm_2O_3 deposition and the reaction conditions have larger effects on the CH_4 conversion, than the Al_2O_3 support properties. The CH_4 conversions (14–16%) for the $\text{Sm}_2\text{O}_3/\text{Al}_2\text{O}_3$ -OM catalysts are consistent with the conversions obtained from the bare supports, while the CH_4 conversions over the $\text{Sm}_2\text{O}_3/\text{Al}_2\text{O}_3$ -IM catalysts are higher (18.5–20.5%). These results suggest that more support is accessible to reaction on the $\text{Sm}_2\text{O}_3/\text{p-Al}_2\text{O}_3$ (OM) catalyst compared with the $\text{Sm}_2\text{O}_3/\text{p-Al}_2\text{O}_3$ (IM) and $\text{Sm}_2\text{O}_3/\text{p-Al}_2\text{O}_3$ (ME) catalysts. The Sm_2O_3 dispersion is thus likely highest on the $\text{Sm}_2\text{O}_3/\text{Al}_2\text{O}_3$ (IM) catalysts and lowest on the $\text{Sm}_2\text{O}_3/\text{p-Al}_2\text{O}_3$ (OM) catalysts.

In contrast, the C_2 selectivity is strongly influenced by the Al_2O_3 support. In most cases, catalysts supported on the more acidic $\text{n-Al}_2\text{O}_3(+)$ exhibit a lower C_2 selectivity than catalysts supported on the $\text{p-Al}_2\text{O}_3$ (Table 2 and Fig. 4). The highest C_2 selectivity of the Al_2O_3 -supported catalysts is obtained over the $\text{Sm}_2\text{O}_3/\text{n-Al}_2\text{O}_3(-)$ -IM catalyst and this is true for all $\text{CH}_4:\text{O}_2$ ratios at both reaction temperatures (Fig. 4). The $\text{Sm}_2\text{O}_3/\text{n-Al}_2\text{O}_3(-)$ -OM also has a higher C_2 selectivity than the other $\text{Sm}_2\text{O}_3/\text{Al}_2\text{O}_3$ -OM catalysts at most conditions (Fig. 5). Considering the higher acidity of the $\text{n-Al}_2\text{O}_3(-)$ support versus the $\text{p-Al}_2\text{O}_3$ support, this result is unexpected, but

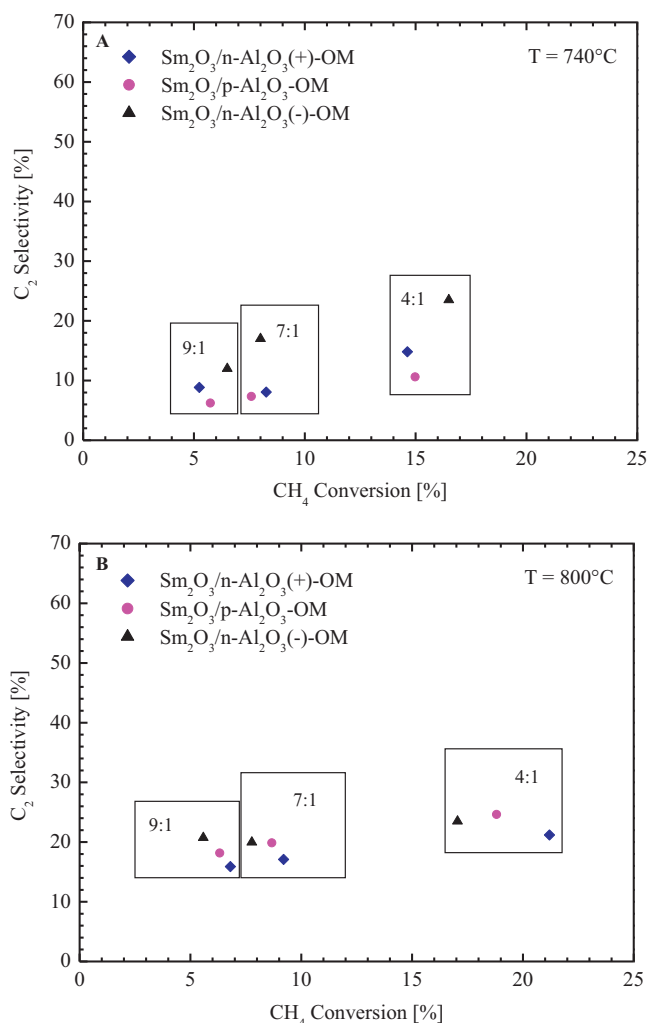


Fig. 4. OCM reaction data for Sm_2O_3 supported on different Al_2O_3 supports prepared using incipient wetness impregnation of a hexane dispersion of Sm_2O_3 (N)-OM nanoparticles. The numbers in the boxes indicate the $\text{CH}_4:\text{O}_2$ feed ratios, i.e. 4:1, 7:1 and 9:1. (A) reaction temperature of 740 °C and (B) reaction temperature of 800 °C.

indicates that other support properties also influence the selectivity. The original surface area can be excluded, as it is similar on the n- $\text{Al}_2\text{O}_3(-)$ and p- Al_2O_3 supports (Table 1). As for the p- Al_2O_3 -supported catalysts, the impregnation method using the nitrate precursor (the $\text{Sm}_2\text{O}_3/\text{n-Al}_2\text{O}_3(-)\text{-IM}$ and $\text{Sm}_2\text{O}_3/\text{n-Al}_2\text{O}_3(+)\text{-IM}$ catalysts) results in catalysts with considerably higher C_2 yields than the catalysts prepared using the $\text{Sm}_2\text{O}_3(\text{N})\text{-OM}$ nanoparticles (the $\text{Sm}_2\text{O}_3/\text{n-Al}_2\text{O}_3(-)\text{-OM}$ and $\text{Sm}_2\text{O}_3/\text{n-Al}_2\text{O}_3(+)\text{-OM}$ catalysts), due to higher CH_4 conversions and C_2 selectivities. This result supports the conclusion that the Sm_2O_3 dispersion is higher on the $\text{Sm}_2\text{O}_3/\text{Al}_2\text{O}_3(\text{IM})$ catalysts compared with the $\text{Sm}_2\text{O}_3/\text{Al}_2\text{O}_3(\text{OM})$ catalysts.

Using the incipient wetness impregnation method of a nitrate precursor onto the Al_2O_3 supports (the $\text{Sm}_2\text{O}_3/\text{Al}_2\text{O}_3\text{-IM}$ catalyst series), the trends in product distribution appear to be similar over the different Al_2O_3 supports. For example, over the $\text{Sm}_2\text{O}_3/\text{p-Al}_2\text{O}_3\text{-IM}$ catalyst at 740 °C the $\text{C}_2\text{H}_4:\text{C}_2\text{H}_6$ product ratio increases from 0.6 to 1.3 and the $\text{CO}_2:\text{CO}$ product ratio increases from 1.8 to 2.4 with decreasing $\text{CH}_4:\text{O}_2$ ratio (Table 3). These trends are expected considering the $\text{CH}_4:\text{O}_2$ stoichiometry of the reactions (CH_4 to C_2H_4 versus C_2H_6 and CH_4 to CO_2 versus CO) and are the same (with similar product ratios) over the other $\text{Sm}_2\text{O}_3/\text{Al}_2\text{O}_3\text{-IM}$ catalysts (not shown). Even at a reaction temperature of 800 °C the

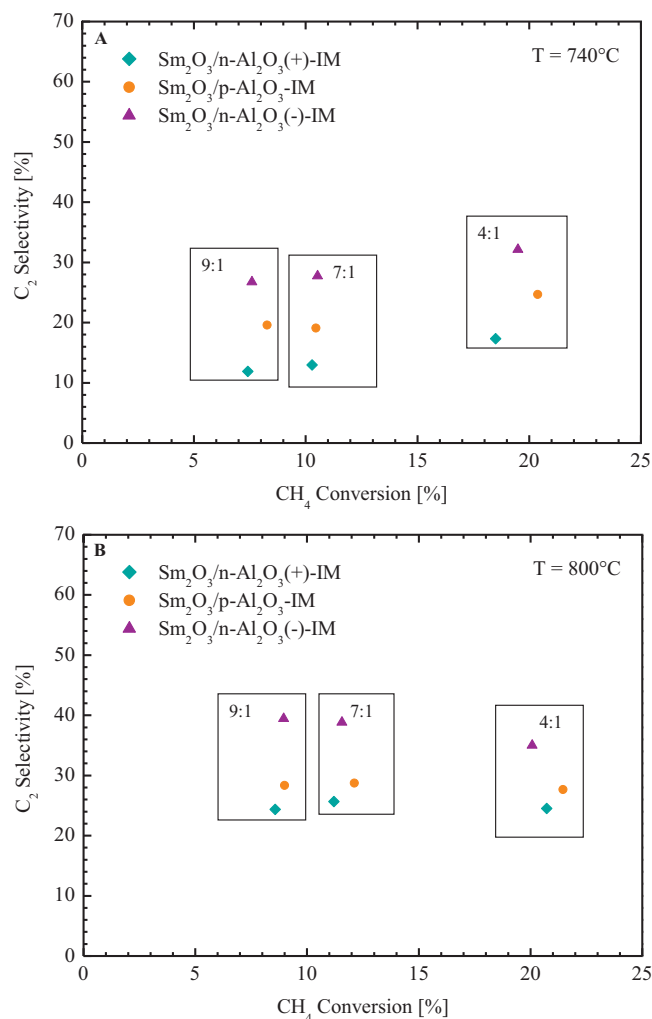


Fig. 5. OCM reaction data obtained from catalysts prepared using incipient wetness impregnation of an aqueous samarium nitrate solution on different Al_2O_3 supports. The numbers in the boxes indicate the $\text{CH}_4:\text{O}_2$ feed ratios, i.e. 4:1, 7:1 and 9:1. (A) reaction temperature of 740 °C and (B) reaction temperature of 800 °C.

trend is the same, only the $\text{C}_2\text{H}_4:\text{C}_2\text{H}_6$ product ratios are higher (for the $\text{Sm}_2\text{O}_3/\text{p-Al}_2\text{O}_3\text{-IM}$ catalyst they increase from 1.3 to 2.7), which is expected over samaria catalysts [6]. The $\text{C}_2\text{H}_4:\text{C}_2\text{H}_6$ and $\text{CO}_2:\text{CO}$ product ratios vary more with Al_2O_3 supports over the $\text{Sm}_2\text{O}_3/\text{Al}_2\text{O}_3\text{-OM}$ catalysts compared with the $\text{Sm}_2\text{O}_3/\text{n-Al}_2\text{O}_3\text{-IM}$ catalysts. For example, the higher $\text{CO}_2:\text{CO}$ product ratio of the $\text{Sm}_2\text{O}_3/\text{n-Al}_2\text{O}_3(-)\text{-OM}$ catalyst compared with the $\text{Sm}_2\text{O}_3/\text{p-Al}_2\text{O}_3\text{-OM}$ catalyst, reflects the higher $\text{CO}_2:\text{CO}$ product ratio of the n- $\text{Al}_2\text{O}_3(-)$ versus the p- Al_2O_3 supports. This again is consistent with more Al_2O_3 being exposed on the OM versus the IM series of catalysts. Thus, the higher CO_2 and CO product concentrations (lower C_2 selectivities), observed over the $\text{Sm}_2\text{O}_3/\text{Al}_2\text{O}_3$ catalysts are due to the Al_2O_3 support. The best Al_2O_3 -supported catalyst is the $\text{Sm}_2\text{O}_3/\text{n-Al}_2\text{O}_3(-)\text{-IM}$, and the main reason is likely that more of the alumina support is covered by Sm_2O_3 on catalysts prepared using impregnation with an aqueous solution of samarium nitrate compared to the other preparation methods. Furthermore, the C_2 selectivity of the n- $\text{Al}_2\text{O}_3(-)$ is slightly higher than that of the p- Al_2O_3 . The $\text{Sm}_2\text{O}_3/\text{n-Al}_2\text{O}_3(-)\text{-IM}$ catalyst can almost compete with the best pure NP samaria catalyst as the best C_2 yield over this catalyst is 5.6% at 800 °C, while it is 7.8% at 740 °C (or 6.8% at 800 °C) over the $\text{Sm}_2\text{O}_3(\text{N})\text{-OM}$ NPs. Since the Sm_2O_3 content is only 20% for the Al_2O_3 -supported catalysts, the amount of C_2 products produced per gram of Sm_2O_3 is more than three times higher over the

Al₂O₃-supported catalysts compared with the pure Sm₂O₃ NPs. Therefore, considering the limited supply of “rare earth oxides”, using an Al₂O₃ support can reduce the amount of REO needed and by modifying the support to, for example, make it more basic, as well as adding alkaline earth promoters to the Sm₂O₃ it should be possible to prepare supported samaria catalysts that can significantly outperform pure Sm₂O₃ catalysts.

3.1.4. Supported Sm₂O₃ catalysts – effects of calcination temperature

The effects of calcination temperature on selected supported catalysts were also investigated by calcining Sm₂O₃/p-Al₂O₃-IM and Sm₂O₃/p-Al₂O₃-ME catalysts at 1000 °C instead of at 800 °C. Tables 2 and 3, reveal that the effects of calcination temperature on the supported Sm₂O₃ catalysts are dependent on the preparation method. For the Sm₂O₃/p-Al₂O₃-ME catalyst there is a significant increase in C₂ selectivity and a slight increase in CH₄ conversion after calcination at the higher temperature (Fig. 2B). This is true at both reaction temperatures, 740 °C and 800 °C, although the percent increase in C₂ yield after the calcination at 1000 °C versus 800 °C is higher at 740 °C. While this trend is similar to that observed over the Sm₂O₃(Cl)-OM NPs, the increase in selectivity is more significant over the Sm₂O₃/p-Al₂O₃-ME catalyst. In contrast, over the Sm₂O₃/p-Al₂O₃-IM catalyst, there is a slight decrease in both CH₄ conversion and C₂ selectivity after calcination at 1000 °C.

While calcination at a higher temperature can be beneficial for Al₂O₃-supported Sm₂O₃ catalysts, it is only under certain circumstances. Therefore, as was the case for the pure Sm₂O₃ NPs, methods other than high temperature treatments are likely to be more effective in improving the catalytic activities and selectivities for Sm₂O₃/Al₂O₃ catalysts.

3.2. Samaria catalyst characterizations

The unsupported samaria NPs and the Sm₂O₃/Al₂O₃ catalysts were subjected to catalyst characterizations to determine properties of importance for the catalytic activities and selectivities and determine differences in these properties as a function of preparation methods and alumina supports used. The results from each technique are presented below.

3.2.1. BET surface area measurements

The BET surface areas of the prepared Sm₂O₃ nanoparticles after calcination at 800 °C are presented in Table 1. The particle sizes calculated using the BET surface areas are included in the table. It is evident from these results that the oleate method gives smaller nanoparticles (larger BET surface area) than the microemulsion method, and, using the oleate method, the NO₃⁻ precursor results in slightly smaller particles compared to the Cl⁻ precursor. The lower BET surface areas do explain the lower activities of the Sm₂O₃(N)-ME and Sm₂O₃(Cl)-OM NPs compared with the Sm₂O₃(N)-OM NPs, but no simple correlation between the BET surface area and the activity or selectivity data obtained over the Sm₂O₃ nanoparticles is evident. For example, the Sm₂O₃(N)-ME NPs are more active than would be expected from their surface area, and the Sm₂O₃(N)-OM NPs have the lowest activity per m² of the Sm₂O₃ NPs even though they are the most active per unit mass. Since the Sm₂O₃ nanoparticles were prepared using different methods, and there are likely residues from the catalyst preparation present on the surface of the NPs (which could cover some of Sm₂O₃), it is not expected that there will be a straight correlation between the catalytic activity and the surface area of these nanoparticles. However, it is also possible that factors other than the Sm₂O₃ surface area are important for a high catalytic activity. The results from the Sm₂O₃(N)-OM NPs calcined at different temperatures indicate that this may be the case. While there

is a significant decrease in surface area from 14.5 m²/g to 1.1 m²/g when increasing the calcination temperature from 800 °C and 1000 °C, this only results in a small decrease in activity (1% ± 0.5%) and this is true for all reaction temperatures and reactant feed ratios. However, there is a significant decrease in the C₂ selectivity at the higher calcination temperature, which indicates that smaller Sm₂O₃ particles (higher Sm₂O₃ surface areas) are beneficial for the reaction.

As expected, due to the high surface areas of the alumina supports, the BET surface areas of the supported Sm₂O₃ catalysts are significantly larger than those of the Sm₂O₃ NPs (Table 1). However, despite the higher original surface area of the n-Al₂O₃(+) support, the catalysts supported on the p-Al₂O₃ exhibit the highest surface areas. The lowest surface area is obtained from catalysts supported on the n-Al₂O₃(-). The p-Al₂O₃ support is therefore more stable than the nanoparticle Al₂O₃ supports during catalyst preparation and the high calcination temperatures (800 °C or higher) used in the investigation. The higher stability of the p-Al₂O₃ support is also evident when comparing catalysts prepared using different methods. The BET surface areas of the Sm₂O₃/p-Al₂O₃ catalysts prepared using the impregnation or microemulsion techniques vary between 125 and 145 m²/g. In contrast, the BET surface areas of Sm₂O₃ catalysts supported on Al₂O₃(+) vary between 80 and 130 m²/g dependent on which impregnation techniques was used (Table 1). The same numbers for the Sm₂O₃/Al₂O₃(-) catalysts are 50 and 85 m²/g.

Comparing the different preparation methods on the same support, it is evident that the incipient wetness impregnation (IWI) method using the nitrate precursor results in catalysts with smaller surface areas compared with those prepared using the same method and the OM NPs. This suggests that the IWI with the nitrate precursor blocks more of the pores in the Al₂O₃ support during the impregnation and drying steps, so that the reactants are exposed to less alumina over this catalyst compared with the IWI using the OM NPs. This is consistent with the conclusions from the reaction experiments over the Sm₂O₃/Al₂O₃-OM catalysts. Despite the large differences in surface areas between catalysts prepared using the same method but different Al₂O₃-supports, and the similar surface areas for catalysts prepared using different methods on the same support, the CH₄ conversion vary more with catalyst preparation method than with the specific Al₂O₃ support. As no strong correlation was observed between the Sm₂O₃ surface area and activity, it is not surprising that the support surface area does not appear to significantly influence the CH₄ conversion.

In contrast, the C₂ selectivity varies with both preparation method and Al₂O₃ support. Although the reason for this is not due to the variation in the overall catalyst surface area, the BET data reveals some interesting properties that are likely important in these reactions. As the alumina can provide acidic sites that promote oxidation to undesired CO_x, optimizing the catalyst synthesis procedure and use of supports that can provide a high surface area for the Sm₂O₃ while at the same time minimize the number of exposed acidic sites are important. The properties of the p-Al₂O₃, n-Al₂O₃(+), and n-Al₂O₃(-) are very different and this is evident in the product distribution from the catalysts on these supports. However, the preparation method can also have a significant effect on the selectivity. Due to the high surface area and the acidity of the n-Al₂O₃(+), the catalysts on this support in general exhibit the lowest C₂ selectivities. However, the lowest C₂ selectivity of all the Al₂O₃-supported catalysts is observed over the Sm₂O₃/p-Al₂O₃-OM catalyst at a reaction temperature of 740 °C. Comparing the catalysts prepared using IWI of OM NPs versus the IWI of the nitrate precursor, it is evident that the OM method results in catalysts with significantly lower C₂ selectivities. The BET surface area measurements indicate that this is due to the fact that more of the Al₂O₃ support is exposed on these catalysts. The incipient wetness

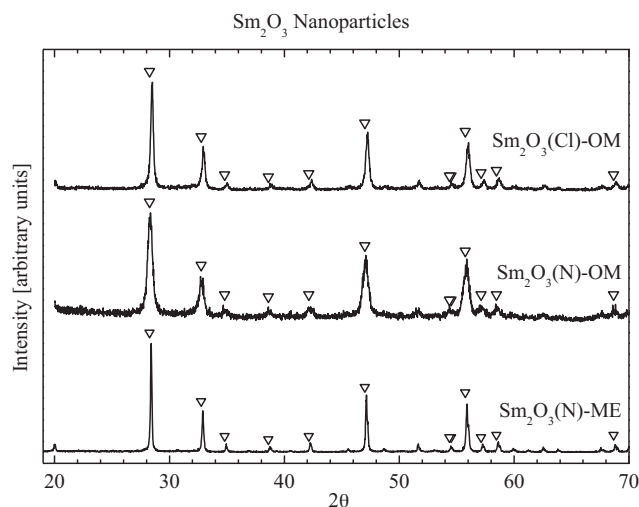


Fig. 6. XRD data obtained from Sm_2O_3 nanoparticles prepared using the oleate decomposition with nitrate and chloride precursors and the reverse microemulsion method using a samarium nitrate precursor. ∇ : indicates peak positions due to cubic Sm_2O_3 .

impregnation using the nitrate precursor appears to block more of the pores on the alumina support compared to the IWI of the OM NPs. The best C_2 selectivities for the supported catalysts are observed over the $\text{Sm}_2\text{O}_3/\text{n-Al}_2\text{O}_3(-)\text{-IM}$ catalyst, and the BET data reveal that this is likely due to the fact that a significant portion of the acidic alumina support has been covered during catalyst preparation.

3.2.2. XRD measurements

The XRD patterns obtained from the NPs synthesized using the microemulsion method ($\text{Sm}_2\text{O}_3(\text{N})\text{-ME}$) after calcination at 800°C is shown in Fig. 6. The main phase identified from the XRD plot is the cubic form of Sm_2O_3 with no major impurities. This is important as the cubic phase has been shown to be more active in the OCM reaction compared with for example the monoclinic phase of Sm_2O_3 [42]. The Sm_2O_3 peaks are well-defined revealing a highly crystalline sample. The average particle size according to the Scherrer equation (Eq. (6)) is 48.2 nm. This is significantly smaller than the particle size estimated from the BET surface area measurement and is likely due to crystal defects in the Sm_2O_3 nanoparticles, which would result in broader XRD peaks. Using the Scherrer equation it is assumed that the line-broadening is due to particle size effects only, and thus resulting in XRD particle sizes that are smaller than the real average particle size. Furthermore, the presence of XRD invisible amorphous Sm_2O_3 cannot be excluded.

The $\text{Sm}_2\text{O}_3(\text{N})\text{-OM}$ NPs yield significantly broader XRD peaks compared to the $\text{Sm}_2\text{O}_3(\text{N})\text{-ME}$ NPs (Fig. 6). This is an indication of smaller particles, as would be expected from the larger BET surface area of the $\text{Sm}_2\text{O}_3(\text{N})\text{-OM}$ compared with the $\text{Sm}_2\text{O}_3(\text{N})\text{-ME}$ NPs. The crystallite size for the $\text{Sm}_2\text{O}_3(\text{N})\text{-OM}$ NPs calculated using the Scherrer equation is 14.0 nm, i.e. significantly smaller than for the $\text{Sm}_2\text{O}_3(\text{N})\text{-ME}$ NPs.

The slightly broadened peaks in the XRD pattern obtained from the $\text{Sm}_2\text{O}_3(\text{Cl})\text{-OM}$ NPs are characteristic of the small grain sizes in the crystalline phase. According to the Scherrer equation, the average crystallite size for the $\text{Sm}_2\text{O}_3(\text{Cl})\text{-OM}$ NPs is approximately 25.4 nm. While the particle sizes determined from the XRD measurements in all cases are smaller than those calculated using the BET surface areas, they do follow the same trend, i.e. the $\text{Sm}_2\text{O}_3(\text{N})\text{-OM}$ are the smallest and the $\text{Sm}_2\text{O}_3(\text{N})\text{-ME}$ are the largest NPs.

The XRD patterns obtained from the $\text{Sm}_2\text{O}_3/\text{p-Al}_2\text{O}_3$ catalysts are presented in Fig. 7A. While the $\text{Sm}_2\text{O}_3(\text{N})\text{-OM}$ NPs are cubic

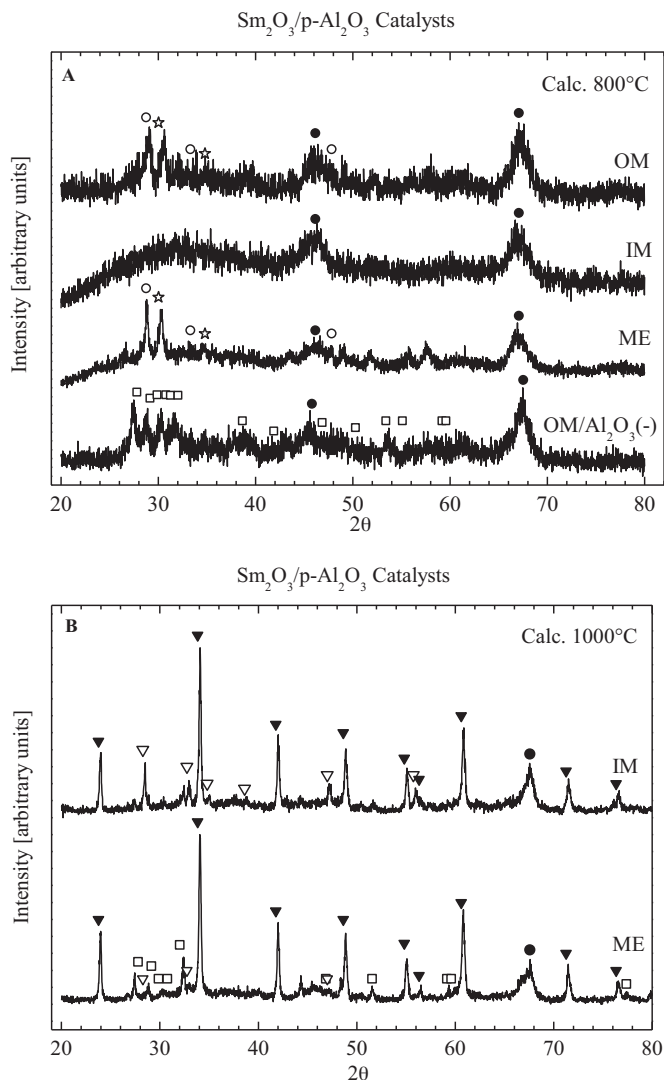


Fig. 7. A) XRD data obtained from the $\text{Sm}_2\text{O}_3/\text{p-Al}_2\text{O}_3\text{-OM}$, $\text{Sm}_2\text{O}_3/\text{p-Al}_2\text{O}_3\text{-IM}$, $\text{Sm}_2\text{O}_3/\text{p-Al}_2\text{O}_3\text{-ME}$ and $\text{Sm}_2\text{O}_3/\text{n-Al}_2\text{O}_3(-)\text{-OM}$ catalysts after calcination at 800°C . B) XRD data obtained from the $\text{Sm}_2\text{O}_3/\text{p-Al}_2\text{O}_3\text{-IM}$ and $\text{Sm}_2\text{O}_3/\text{p-Al}_2\text{O}_3\text{-ME}$ catalysts after calcination at 1000°C . \square : monoclinic Sm_2O_3 , \circ : Sm_2O_3 , \ast : $\text{SmO}_{0.656}$, \bullet : $\gamma\text{-Al}_2\text{O}_3$, \blacktriangledown : SmAlO_3 , and \triangle : cubic Sm_2O_3 .

after calcination at 800°C , in the presence of the Al_2O_3 support the cubic Sm_2O_3 appears to undergo a transformation, as no peak due to cubic Sm_2O_3 is visible in the XRD pattern obtained from the $\text{Sm}_2\text{O}_3/\text{p-Al}_2\text{O}_3$ catalysts and the Sm_2O_3 is evidently less crystalline on the $\text{Sm}_2\text{O}_3/\text{p-Al}_2\text{O}_3$ catalysts. In addition to the broad peaks due to the poorly crystalline $\gamma\text{-Al}_2\text{O}_3$ support, the XRD patterns obtained from the $\text{Sm}_2\text{O}_3/\text{p-Al}_2\text{O}_3\text{-ME}$ and $\text{Sm}_2\text{O}_3/\text{p-Al}_2\text{O}_3\text{-OM}$ catalysts exhibit two peaks near $2\theta = 30^\circ$. In contrast, the $\text{Sm}_2\text{O}_3/\text{n-Al}_2\text{O}_3(-)\text{-OM}$ catalyst exhibits four peaks in this region. The differences in the XRD patterns obtained from the $\text{Sm}_2\text{O}_3/\text{p-Al}_2\text{O}_3\text{-OM}$ and $\text{Sm}_2\text{O}_3/\text{n-Al}_2\text{O}_3(-)\text{-OM}$ catalysts, suggest that the interactions between the Sm_2O_3 and the Al_2O_3 are different on the $\text{p-Al}_2\text{O}_3$ and $\text{n-Al}_2\text{O}_3$ supports. While the presence of monoclinic Sm_2O_3 cannot be ruled out on these catalysts, particularly not on the $\text{Sm}_2\text{O}_3/\text{n-Al}_2\text{O}_3(-)\text{-OM}$ catalyst, the reference monoclinic Sm_2O_3 peaks (JCPDS [42–1464]) are not a good match (Fig. 7A). The peaks are not due to fully developed mixed metal oxide phases either, such as SmAlO_3 or $\text{Sm}_4\text{Al}_2\text{O}_9$ [39,43]. However, these peaks have been observed on a 40% Sm_2O_3 on Al_2O_3 catalyst [39], and may thus be a precursor to SmAlO_3 formation, or they could be due to Sm-rich SmO_x (Fig. 7A). The fact that the XRD pattern obtained

from a spent catalyst (not shown), after several hours on stream, only shows particle size growth and does not contain any peaks due to SmAlO_3 suggests that the peaks most likely are due to Sm-rich SmO_x .

No peaks due to Sm_2O_3 are observed in the XRD pattern obtained from the $\text{Sm}_2\text{O}_3/\text{p-Al}_2\text{O}_3$ -IM catalyst. Thus, the incipient wetness impregnation using the nitrate precursor, results in Sm_2O_3 on the surface which is either amorphous or has particle sizes below the detection limit of XRD. While it is possible that the inferior performance of the Al_2O_3 -supported catalysts compared with the Sm_2O_3 NPs is due to the change in Sm_2O_3 crystal phase, it is more likely that the lower activity and selectivity are due to the lower Sm_2O_3 content and the acidic alumina, respectively, on the $\text{Sm}_2\text{O}_3/\text{p-Al}_2\text{O}_3$ catalysts.

After calcination at 1000°C , the $\text{Sm}_2\text{O}_3/\text{p-Al}_2\text{O}_3$ -IM and $\text{Sm}_2\text{O}_3/\text{p-Al}_2\text{O}_3$ -ME catalysts are much more crystalline (Fig. 7B). While some peaks due to $\gamma\text{-Al}_2\text{O}_3$ and cubic Sm_2O_3 can be observed in the XRD patterns from these catalysts, the main crystalline phase is a samarium aluminum oxide (SmAlO_3) [41]. Even though the transformation from poorly crystalline $\text{Sm}_2\text{O}_3/\gamma\text{-Al}_2\text{O}_3$ to SmAlO_3 appears to be similar on both catalysts, the behavior of the $\text{Sm}_2\text{O}_3/\text{p-Al}_2\text{O}_3$ -IM and $\text{Sm}_2\text{O}_3/\text{p-Al}_2\text{O}_3$ -ME catalysts with calcination temperature is very different. This could be due to two opposing effects, i.e. SmAlO_3 formation decreases the surface Al_2O_3 concentration (a positive effect), but it also decreases the Sm_2O_3 at the surface (a negative effect). On the $\text{Sm}_2\text{O}_3/\text{p-Al}_2\text{O}_3$ -IM the high-temperature treatment causes particle growth and/or crystallization of the cubic Sm_2O_3 phase. The lower activity on the

$\text{Sm}_2\text{O}_3/\text{p-Al}_2\text{O}_3$ -IM catalyst after calcination at 1000°C is therefore likely due to a lower Sm_2O_3 surface area, due to both SmAlO_3 formation and Sm_2O_3 particle growth. In contrast, the $\text{Sm}_2\text{O}_3/\text{p-Al}_2\text{O}_3$ -ME catalyst after calcination appears to consist of other SmO_x phases in addition to the cubic Sm_2O_3 . The effects of these SmO_x phases on the catalytic activity and selectivity are not known, but they do not appear to be detrimental. It is also possible that the calcination treatment removes (or redistributes) residues that are left from the catalyst preparation procedure, residues which could have resulted in the low initial activity and selectivity observed over this catalyst after calcination at 800°C .

3.2.3. TEM analysis

TEM images obtained from the $\text{Sm}_2\text{O}_3(\text{N})$ -OM NPs before the calcination step is presented in Fig. 8A. Small nanoparticles with diameters between 3 and 5 nm and a narrow size distribution are observed. After calcination at 800°C particle agglomeration is evident, but there are still particles present with diameters around 5 nm (Fig. 8B). However, significantly larger particles are also present and, thus, the particle size distribution is significantly broader. The particle sizes appear to be reasonably consistent with the 14 nm average crystallite size determined from the XRD data, but there is significant agglomeration which explains the larger particle size obtained from the BET surface area measurements.

The TEM image for the $\text{Sm}_2\text{O}_3(\text{N})$ -ME NPs (post calcination) reveal highly crystalline NPs with a particle size range between 30 and 50 nm (Fig. 8C). Thus, these particles are larger than

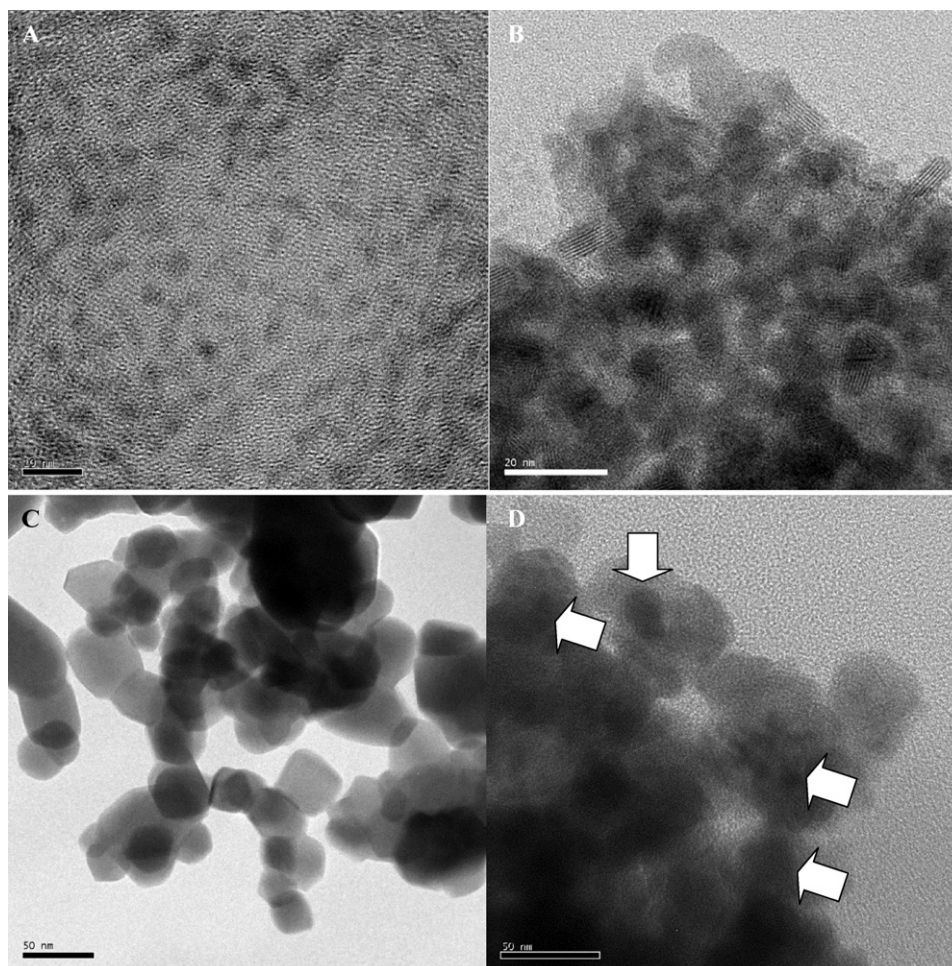


Fig. 8. TEM images obtained from (A) $\text{Sm}_2\text{O}_3(\text{N})$ -OM NPs before calcination (scale bar = 10 nm), (B) $\text{Sm}_2\text{O}_3(\text{N})$ -OM NPs after calcination at 800°C (scale bar = 20 nm), (C) $\text{Sm}_2\text{O}_3(\text{N})$ -ME NPs after calcination at 800°C (scale bar = 50 nm), and (D) $\text{Sm}_2\text{O}_3/\text{n-Al}_2\text{O}_3(-)$ -OM catalyst after calcination at 800°C (scale bar = 50 nm).

the $\text{Sm}_2\text{O}_3(\text{N})\text{-OM}$ NPs, but appears to be less agglomerated after calcination. The particle sizes from TEM is fairly consistent with the average particle size calculated using the XRD data, but there are significantly larger particles present which again explains the particle size determined from the BET surface area.

The TEM image of the $\text{Sm}_2\text{O}_3(\text{N})\text{-OM}$ NPs deposited onto the alumina support reveal reasonably small Sm_2O_3 particles dispersed on the surface of the $\text{n-Al}_2\text{O}_3(-)$ support. Due to the difference in the material (samaria is a high Z material, while alumina is a low Z material), it is possible distinguish between the two oxides (Fig. 8D).

3.2.4. XPS measurements

XPS spectra were collected from the three Sm_2O_3 catalysts supported on the $\text{p-Al}_2\text{O}_3$ to determine the effects of catalyst

preparation method on the supported catalysts. The survey spectra are presented in Fig. 9A. To facilitate analysis, the high binding energy region between 1200 and 900 eV, and the low binding energy region between 500 and 0 eV are displayed in Fig. 9B and C, respectively. The main differences between the catalysts are variations in the relative peak intensities. The $\text{Sm}_2\text{O}_3/\text{p-Al}_2\text{O}_3\text{-IM}$ has the lowest carbon content. The higher carbon content on the other catalysts is likely due to residual carbon on the surface from the catalyst preparation, i.e. from the oleate complex for the $\text{Sm}_2\text{O}_3/\text{p-Al}_2\text{O}_3\text{-OM}$ and from the Tween 80 surfactant for the $\text{Sm}_2\text{O}_3/\text{p-Al}_2\text{O}_3\text{-ME}$ catalyst. On a carbon-free basis, or looking only at the Al, Sm and O peaks, the Sm/Al and O/(Sm + Al) peak area ratios are similar for the $\text{Sm}_2\text{O}_3/\text{p-Al}_2\text{O}_3\text{-ME}$ and $\text{Sm}_2\text{O}_3/\text{p-Al}_2\text{O}_3\text{-IM}$ catalysts (Table 4). Perhaps the most important difference between the three catalysts is the higher Sm/Al

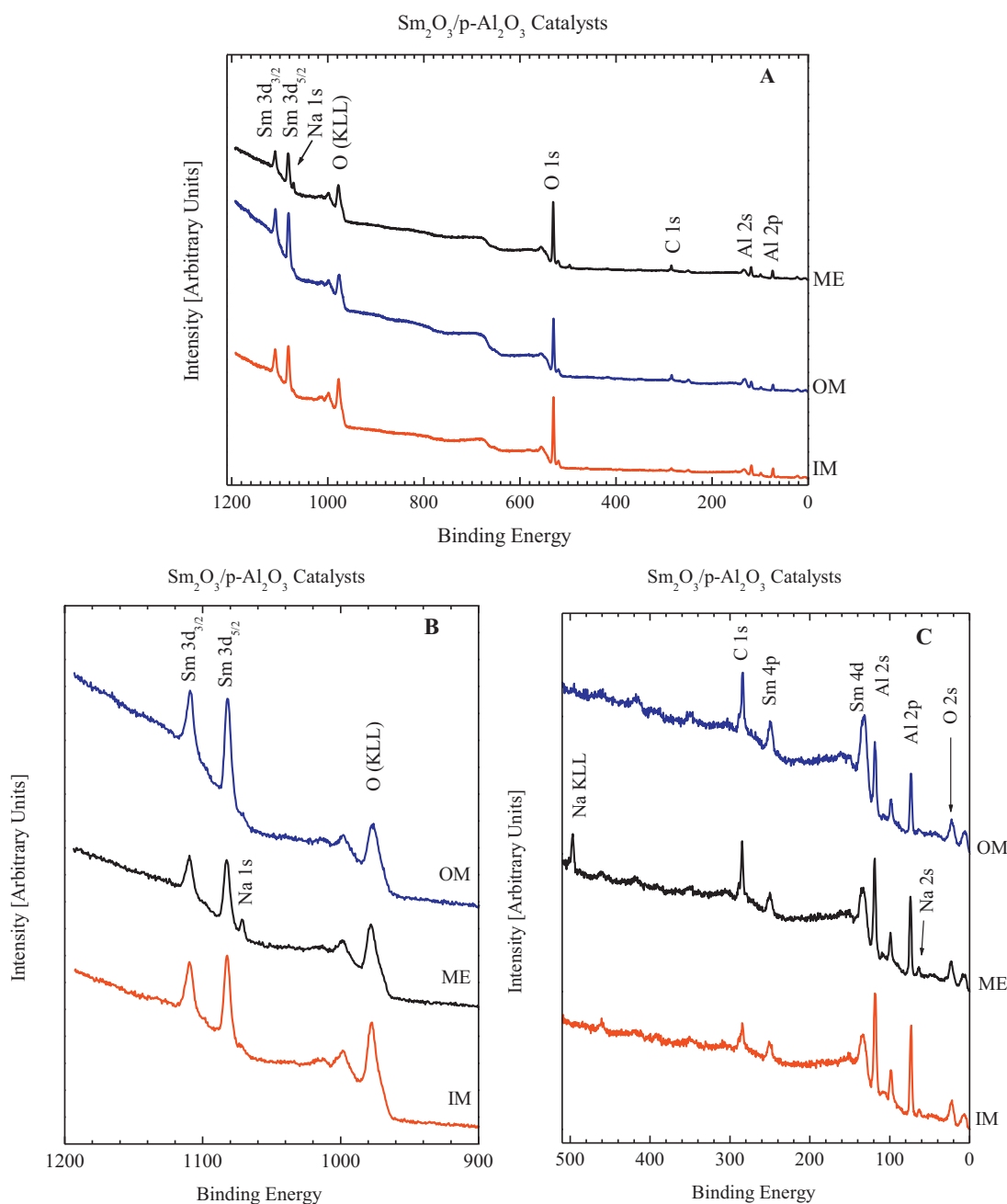


Fig. 9. XPS survey spectra obtained from the $\text{Sm}_2\text{O}_3/\text{p-Al}_2\text{O}_3\text{-IM}$, $\text{Sm}_2\text{O}_3/\text{p-Al}_2\text{O}_3\text{-OM}$ and $\text{Sm}_2\text{O}_3/\text{p-Al}_2\text{O}_3\text{-ME}$ catalysts. (A) Full scale XPS survey spectra, (B) high binding energy region, and (C) low binding energy region.

Table 4
XPS Compositional analysis obtained from $\text{Sm}_2\text{O}_3/\text{p-Al}_2\text{O}_3$ catalyst series.

Catalyst ^a	O 1s [%]	Sm 3d _{5/2} [%]	Al 2p _{3/2} [%]	C 1s [%]	Na 1s [%]	Sm/Al Ratio	O/(Sm + Al) Ratio
$\text{Sm}_2\text{O}_3(\text{N})/\text{p-Al}_2\text{O}_3\text{-OM}$	57	11	20	12	–	0.55	1.84
$\text{Sm}_2\text{O}_3(\text{N})/\text{p-Al}_2\text{O}_3\text{-ME}$	58	7	23	11	1.5	0.30	1.96
$\text{Sm}_2\text{O}_3(\text{N})/\text{p-Al}_2\text{O}_3\text{-IM}$	63	7	24	6	–	0.29	2.03

^a The following atomic sensitivity factors were used in the calculation of the composition: O 1s=0.711, Sm 3d_{5/2}=2.907, Al 2p=0.193, C 1s=0.296, Na 1s 1.685 [44].

peak area ratio observed on the $\text{Sm}_2\text{O}_3/\text{p-Al}_2\text{O}_3\text{-OM}$ catalyst. Thus, there is more Sm_2O_3 in the near surface region on this catalyst compared with the other $\text{Sm}_2\text{O}_3/\text{p-Al}_2\text{O}_3$ catalysts. This is not necessarily due to a higher Sm_2O_3 surface area on the $\text{Sm}_2\text{O}_3/\text{p-Al}_2\text{O}_3\text{-OM}$ catalyst, as it may simply mean that more Sm_2O_3 is deposited onto the outermost surface of the $\text{p-Al}_2\text{O}_3$ support. The lower intensity of the Al peaks obtained from this catalyst, compared to the $\text{Sm}_2\text{O}_3/\text{p-Al}_2\text{O}_3\text{-IM}$ and $\text{Sm}_2\text{O}_3/\text{p-Al}_2\text{O}_3\text{-ME}$ catalysts, supports this conclusion (Fig. 9 C). This is also consistent with the BET surface area measurements on the $\text{Sm}_2\text{O}_3/\text{p-Al}_2\text{O}_3\text{-OM}$ and $\text{Sm}_2\text{O}_3/\text{p-Al}_2\text{O}_3\text{-IM}$ catalysts. It is possible that the $\text{Sm}_2\text{O}_3(\text{N})\text{-OM}$ NPs do not enter the pores of the $\text{p-Al}_2\text{O}_3$ as efficiently as the aqueous solutions of samarium nitrate in the $\text{Sm}_2\text{O}_3/\text{p-Al}_2\text{O}_3\text{-IM}$ and $\text{Sm}_2\text{O}_3/\text{p-Al}_2\text{O}_3\text{-ME}$ catalysts. So, while the outermost surface has more Sm_2O_3 exposed, the small pores of the alumina support may have more alumina exposed, which would be accessible to gas phase methane and oxygen. This in turn would explain the poor selectivity of this and the other $\text{Sm}_2\text{O}_3/\text{Al}_2\text{O}_3\text{-OM}$ catalysts compared with the $\text{Sm}_2\text{O}_3/\text{p-Al}_2\text{O}_3\text{-IM}$ and $\text{Sm}_2\text{O}_3/\text{p-Al}_2\text{O}_3\text{-ME}$ catalysts. The lowest Sm peak intensities are observed over the $\text{Sm}_2\text{O}_3/\text{p-Al}_2\text{O}_3\text{-ME}$ catalyst and this is mainly due to the presence of sodium on the surface of this catalyst. More residual sodium (from the catalyst preparation) is present on the surface of this catalyst compared to the other $\text{Sm}_2\text{O}_3/\text{p-Al}_2\text{O}_3$ catalysts. While the Sm/Al ratio in the near surface region is similar on the $\text{Sm}_2\text{O}_3/\text{p-Al}_2\text{O}_3\text{-IM}$ and $\text{Sm}_2\text{O}_3/\text{p-Al}_2\text{O}_3\text{-ME}$ catalysts, it is possible that the Na covers both Sm_2O_3 and Al_2O_3 on the $\text{Sm}_2\text{O}_3/\text{p-Al}_2\text{O}_3\text{-ME}$ catalyst. The lower Sm peak intensities in the survey spectrum

obtained from the $\text{Sm}_2\text{O}_3/\text{p-Al}_2\text{O}_3\text{-ME}$ catalyst indicate that this is the case. As alkaline earth metal ions often are used to promote Sm_2O_3 -based OCM catalysts, this is likely the reason why the $\text{Sm}_2\text{O}_3/\text{p-Al}_2\text{O}_3\text{-ME}$ catalyst has the highest C_2 selectivity of the Sm_2O_3 catalysts supported on $\text{p-Al}_2\text{O}_3$. However, the large amount of Na on the surface of this catalyst probably blocks some of the Sm_2O_3 , which would explain the lower CH_4 conversion compared with the $\text{Sm}_2\text{O}_3/\text{p-Al}_2\text{O}_3\text{-IM}$ catalyst. It is likely that the heat treatment at 1000°C immobilizes the Na and causes a redistribution of the Na on the surface of the $\text{Sm}_2\text{O}_3/\text{p-Al}_2\text{O}_3\text{-ME}$ catalyst, so that more Sm_2O_3 is present at the outermost surface compared with before the heat treatment. This together with a potential promoting effect of the Na on the Sm_2O_3 can explain the improved performance of this catalyst after calcination at 1000°C .

The high-resolution XPS scans of the Sm 3d_{5/2} and O 1s regions are shown in Fig. 10A and B, respectively. The Sm 3d_{5/2} binding energy of 1083.0 eV is within the reported range [44]. The Sm 3d_{5/2} peak obtained from the $\text{Sm}_2\text{O}_3/\text{p-Al}_2\text{O}_3\text{-IM}$ catalyst is slightly broader than the Sm 3d_{5/2} peaks obtained from the other $\text{Sm}_2\text{O}_3/\text{p-Al}_2\text{O}_3$ catalysts. This is due to an increased intensity at higher binding energy and could indicate stronger interactions with the alumina support on this catalyst. The O 1s binding energy of 531.3 eV is expected for O 1s in Al_2O_3 . All O 1s peaks are slightly broadened on the high binding energy side, revealing presence of surface hydroxyl groups and possibly carbonate species. The presence of carbonate species is expected over rare earth oxide catalysts.

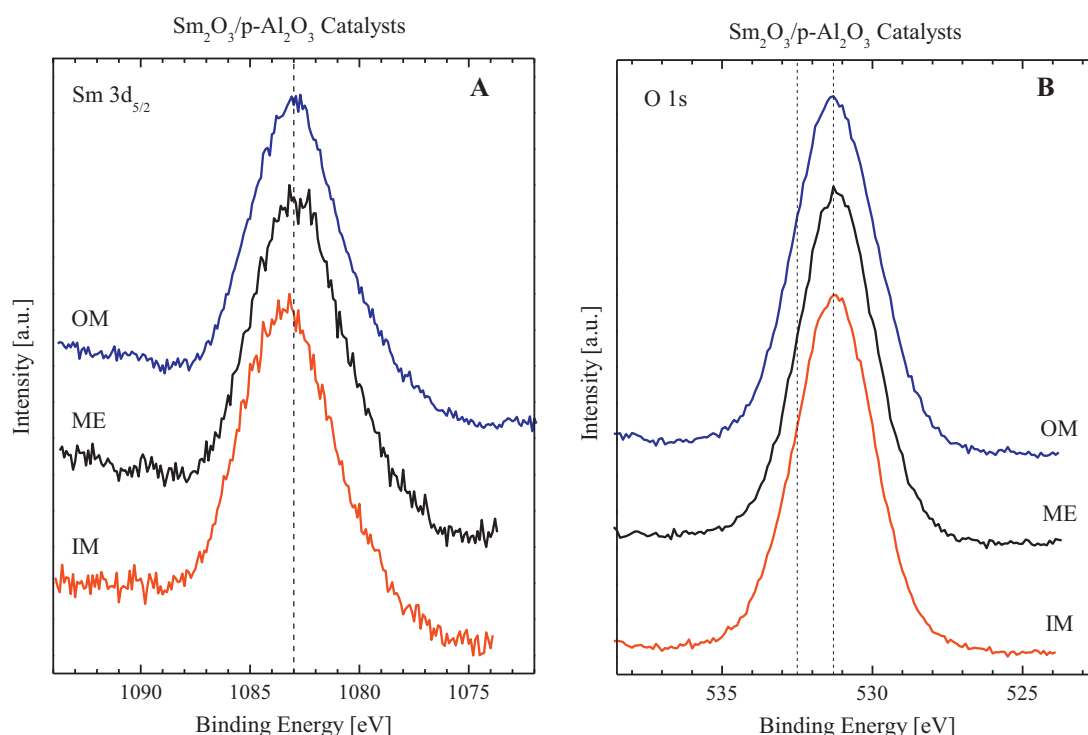


Fig. 10. High-resolution XPS spectra of the (A) Sm 3d_{5/2} and (B) O 1s peaks obtained from the $\text{Sm}_2\text{O}_3/\text{p-Al}_2\text{O}_3\text{-IM}$, $\text{Sm}_2\text{O}_3/\text{p-Al}_2\text{O}_3\text{-OM}$ and $\text{Sm}_2\text{O}_3/\text{p-Al}_2\text{O}_3\text{-ME}$ catalysts.

4. Conclusion

The reaction data obtained from the Sm₂O₃ NPs reveal that the smaller particle sizes of the Sm₂O₃(N)-OM NPs result in higher CH₄ conversions and C₂ selectivities at nearly all conditions used in the investigation. The highest C₂ yield obtained over this catalyst was 7.8% at a CH₄:O₂ ratio of 4:1 and a reaction temperature of 740 °C with a GHSV of 880 h⁻¹. This is not an impressive yield, but it can be significantly improved using typical dopants, such as alkaline earth metals. While several catalysts can produce a reaction yield greater than that obtained over samaria, it remains one of the best performing single compound OCM catalysts [9]. Calcination of pure Sm₂O₃ NPs at 1000 °C instead of 800 °C results in particle sintering and thus a lower surface area with a concomitant reduction in both activity and selectivity. Only under certain conditions, and if the catalyst is prepared using a chloride precursor, is there a positive effect from a higher calcination temperature, but the best performing catalyst is still the Sm₂O₃(N)-OM NPs prepared using a nitrate precursor.

As rare earth oxides are in limited supply, finding ways to minimize the samaria content in a catalyst while still maintaining the benefits of the pure compound are of great interest. While a typical Al₂O₃ support is not expected to yield highly selective catalysts, they are readily available with high surface areas. Therefore, three different Al₂O₃ supports with varying properties were investigated to determine if Al₂O₃ is a viable support. The Al₂O₃-supported catalysts do exhibit a lower C₂ selectivity, likely due to participation from acidic sites on the support, which increases CO_x formation. In particular, there is significantly more CO produced over the supported catalysts compared with the Sm₂O₃ NPs. The catalyst preparation method appears to influence the CH₄ conversion more than the specific Al₂O₃ support used, despite significant differences between the Al₂O₃ support surface areas and acidic and basic properties. In contrast, the C₂ selectivity depends on both the catalyst preparation method and the Al₂O₃ support used. The best supported catalyst is obtained by impregnating the n-Al₂O₃(-) support with an aqueous solution of samarium nitrate. As the C₂ selectivity increases with reaction temperature between 740 °C and 800 °C over the supported catalysts, the highest C₂ yield is obtained at a CH₄:O₂ ratio of 4:1 and a temperature of 800 °C. The impregnation method using the nitrate precursor likely yields the smallest Sm₂O₃ particles on the surface of the Al₂O₃ supports, while at the same time blocking a significant portion of the highly acidic, CO_x producing, alumina sites. The CH₄ conversion over the Sm₂O₃/Al₂O₃(-) catalyst is the same as over the Sm₂O₃(N)-OM (the best performing pure Sm₂O₃ NP catalyst), but the C₂ selectivity is slightly lower. While the C₂ yield per gram of catalyst is lower for the supported catalysts, the C₂ yield per gram of Sm₂O₃ is higher over several of the Al₂O₃-supported catalysts. Therefore, by selectively blocking some of the acidic support sites, it will be possible to increase the C₂ selectivity and thus make the catalysts even more effective per unit weight of Sm₂O₃, and render Al₂O₃ a viable catalyst support for the oxidative coupling of methane.

Acknowledgements

The authors gratefully acknowledge NSF support (Chemistry 1026712). Dr. Valentin Craciun and Dr. Eric Lambers are also

acknowledged for their support during the XRD and XPS measurements and Mr Gill Brubaker for support during the BET surface area measurements. These analyses were performed at the Major Analytical Instrumentation Center (MAIC) and the Particle Engineering Research Center (PERC) at the University of Florida.

References

- [1] S. Liu, F. Chen, S. Xie, P. Zeng, X. Du, L. Xu, J. Nat. Gas Chem. 18 (2009) 21–24.
- [2] J. Orejas, Chem. Eng. Sci. 56 (2001) 513–522.
- [3] W. Liu, A. Eliyas, L. Petrov, Appl. Catal. 61 (1990) 265–274.
- [4] H. Cai, A. Krzywicki, M. Oballa, Chem. Eng. Proc. Process Intensification 41 (2002) 199–214.
- [5] G.E. Keller, M.M. Bhasin, J. Catal. 73 (1982) 9–19.
- [6] K. Otsuka, K. Jinno, A. Morikawa, J. Catal. 100 (1986) 353–359.
- [7] T. Ito, J.H. Lunsford, Nature 314 (1985) 721–722.
- [8] K. Fujimoto, K. Omata, J. Yoshihara, Appl. Catal. 67 (1991) L21–L24.
- [9] O. Forlani, S. Rossini, Mater. Chem. Phys. 31 (1992) 155–158.
- [10] H.B. Zhang, G.D. Lin, H.L. Wan, Y.D. Liu, W.Z. Weng, J.X. Cai, Y.F. Shen, K.R. Tsai, Catal. Lett. 73 (2001) 141–147.
- [11] D.J. Driscoll, W. Martir, J.X. Wang, J.H. Lunsford, J. Am. Chem. Soc. 107 (1985) 58.
- [12] D. Wang, M.P. Rosynek, J.H. Lunsford, J. Catal. 151 (1995) 155–167.
- [13] J.B. Kimble, J.H. Kolts, Energy Prog. 6 (1986) 226–229.
- [14] K. Aika, T. Moriyama, N. Takasaki, E. Iwamatsu, J. Chem. Soc. Chem. Commun. (1986) 1210–1211.
- [15] E. Iwamatsu, T. Moriyama, N. Takasaki, K. Aika, J. Chem. Soc. Chem. Commun. (1987) 19–20.
- [16] T. Moriyama, N. Takasaki, E. Iwamatsu, K. Aika, Chem. Lett. (1986) 1165–1168.
- [17] N. Yamagata, K. Tanaka, S. Sakaki, Z. Okazaki, Chem. Lett. (1987) 81–82.
- [18] W. Hinsen, W. Bytyn, M. Baerns, Proc. Eight Int. Congress Catal. 3 (1984) 581–592.
- [19] J.P. Bartek, J.M. Hupp, J.F. Brazdil, R.K. Grasselli, Catal. Today 3 (1988) 117–126.
- [20] K. Asami, S. Hashimoto, T. Shikada, K. Fujimoto, H. Tominaga, Ind. Eng. Chem. Res. 26 (1987) 1485–1488.
- [21] M.Y. Lo, S.K. Agarwal, G. Marcelin, J. Catal. 112 (1988) 168–175.
- [22] S.K. Agarwal, R.A. Migone, G. Marcelin, Appl. Catal. 53 (1989) 71–80.
- [23] K.D. Campbell, H. Zhang, J.H. Lunsford, J. Phys. Chem. 92 (1988) 750–753.
- [24] J.M. Deboy, R.F. Hicks, J. Catal. 113 (1988) 517–524.
- [25] A.M. Gaffney, C.A. Jones, J.J. Leonard, J.A. Sofranko, J. Catal. 114 (1988) 422–432.
- [26] H.L. Wan, X.P. Zhou, W.Z. Weng, R.Q. Long, Z.S. Chao, W.D. Zhang, M.S. Chen, J.Z. Luo, S.Q. Zhou, Catal. Today 51 (1999) 161–175.
- [27] T. Baidya, N. van Vegten, Y. Jiang, F. Krumeich, A. Baiker, Appl. Catal. A 391 (2011) 205–214.
- [28] K. Otsuka, K. Jinno, A. Morikawa, Chem. Lett. (1985) 499–500.
- [29] K. Otsuka, K. Jinno, Inorg. Chem. Acta 121 (1986) 237–241.
- [30] K. Otsuka, T. Komatsu, Chem. Lett. (1987) 483–484.
- [31] J.A. Labinger, K.C. Ott, J. Phys. Chem. 91 (1987) 2682–2684.
- [32] H. Imai, T. Tagawa, J. Chem. Soc. Chem. Commun. (1986) 52–53.
- [33] K.P. Peil, James G. Goodwin Jr., G. Marcelin, J. Am. Chem. Soc. 112 (1990) 6129–6130.
- [34] M.P. Rosynek, Catal. Rev. - Sci. Eng. 16 (1977) 111–154.
- [35] K.R. Tsai, D.A. Chen, H.L. Wan, H.B. Zhang, G.D. Lin, P.X. Zhang, Catal. Today 51 (1999) 3–23.
- [36] K.R. Tsai, H.B. Zhang, G.D. Lin, H.L. Wan, Y.D. Liu, W.Z. Weng, J.X. Cai, Y.F. Shen, Abstracts of Papers CATL 028, ACS Nat. Mtg., Boston, 1998.
- [37] S.V. Mahajan, J.H. Dickerson, Nanotechnology 18 (2007) 32605–32610.
- [38] W. Zhu, L. Xu, J. Ma, R. Yang, Y. Chen, J. Colloid Interface Sci. 340 (2009) 119–125.
- [39] S.D. Jones, L.M. Neal, H.E. Hagelin-Weaver, Appl. Catal. B 84 (2008) 631–642.
- [40] S.D. Jones, Activity and Characterization Studies in Methanol Reforming Catalysis: Cu and Cu-ZnO Catalysts and the Role of Nanomaterials, Dissertation, 2008.
- [41] M.J. Capitan, P. Malet, M.A. Centeno, A. Munoz-Paez, I. Carrizosa, J.A. Odriozola, J. Phys. Chem. 97 (1993) 9233–9249.
- [42] S.N. Vereshchagin, J.R.H. Ross, Catal. Today 24 (1995) 285–287.
- [43] C.L. Huang, Y.C. Chen, Mater. Res. Bull. 37 (2002) 563–574.
- [44] J.F. Moulder, W.F. Stickle, P.E. Sobol, K.D. Bomben, Handbook of X-Ray Photoelectron Spectroscopy, Eden Prairie, Minnesota, 1995.